DESIGN AND DEVELOPMENT OF NOVEL FIN MICRO-CHANNEL HEAT SINK FOR HIGH HEAT FLUX APPLICATION

By

NOR HAZIQ NAQIUDDIN BIN HAMLI

A dissertation submitted to the Department of Mechanical and Material Engineering,
Lee Kong Chian Faculty of Engineering and Science,
Universiti Tunku Abdul Rahman,
in partial fulfillment of the requirements for the degree of
Master of Engineering Science
February 2019

ABSTRACT

DESIGN AND DEVELOPMENT OF NOVEL FIN MICRO-CHANNEL HEAT SINK FOR HIGH HEAT FLUX APPLICATION

The scale-down trend increases the chips' density and the high power handling capability generates unnecessary heat which can disrupt the reliability of the electronic devices. Therefore, various types of cooling solution have been proposed to enhance heat dissipation from electronic devices. One of the solutions is using an inexpensive straight-channel heat sink. However, the presence of a large temperature gradient between the upstream and downstream in the straight-channel can shorten the life span of the device and subsequently reduce the reliability. In this work, a novel segmented micro-channel is introduced to improve the thermal performance of the straight-channel heat sink. Computational fluid dynamic analysis is performed to investigate the performance of the micro-channel heat sink. Next, Taguchi-grey method is applied to optimize the design of the segmented micro-channel. The results indicate that three segments of the segmented micro-channel, fin width-1 mm, fin length-2 mm, fin transverse distance-5 mm and channel width-1 mm is an optimized design of the segmented micro-channel with enhanced heat transfer performance and minimum pressure drop. It is also found that the optimized micro-channel heat sink is able to cool the chip with a heat flux of 800 W to 56.6 ^{o}C and pumping power of 0.13 W using 15 gs^{-1} of water. Experimental work shows that the result deviates less than 5% for average temperature and temperature variation at 15 gs^{-1}.

ACKNOWLEDGEMENTS

I would like to thank everyone who had contributed to the successful completion of this research work. I would like to express my gratitude to my research supervisor, Dr. Bernard Saw Lip Huat and my co-supervisor, Dr. Yew Ming Chian for his invaluable advice, guidance and his enormous patience throughout the development of the research work.

In addition, I would also like to express my gratitude to my loving parents and friends who had helped and given me encouragement to continue to complete this research work without any problem or delay. Lastly, I would thank Universiti Tunku Abdul Rahman which given me the opportunity to take part in doing this research work with the facilities provided by them.

APPROVAL SHEET

This dissertation entitled "**DESIGN AND DEVELOPMENT OF NOVEL FIN MICRO-CHANNEL HEAT SINK FOR HIGH HEAT FLUX APPLICATION"** was prepared by NOR HAZIQ NAQIUDDIN BIN HAMLI and submitted as partial fulfillment of the requirements for the degree of Master of Engineering Science at Universiti Tunku Abdul Rahman.

Approved by:

_____
(Dr. Bernard Saw Lip Huat)
Date:……..
Supervisor
Department of Mechanical and Material Engineering
Lee Kong Chian Faculty of Engineering and Science
Universiti Tunku Abdul Rahman

_____
(Dr. Yew Ming Chian)
Date:……..
Co-supervisor
Department of Mechanical and Material Engineering
Lee Kong Chian Faculty of Engineering and Science
Universiti Tunku Abdul Rahman

LEE KONG CHIAN FACULTY OF ENGINEERING AND SCIENCE

UNIVERSITI TUNKU ABDUL RAHMAN

Date:

SUBMISSION OF DISSERTATION

It is hereby certified that Nor Haziq Naqiuddin Bin Hamli (ID No: 16UEM07629) has completed this dissertation entitled "*Design and development of novel fin micro-channel for high heat flux application*" under the supervision of Dr. Bernard Saw Lip Huat (Supervisor) from the Department of Mechanical and Material Engineering, Lee Kong Chian Faculty of Engineering and Science, and Dr. Yew Ming Chian (Co-Supervisor) from the Department of Mechanical and Material Engineering, Lee Kong Chian Faculty of Engineering.

I understand that University will upload softcopy of my dissertation in pdf format into UTAR Institutional Repository, which may be made accessible to UTAR community and the public.

Yours truly,

_____

(*NOR HAZIQ NAQIUDDIN BIN HAMLI*)

DECLARATION

I hereby declare that the dissertation is based on my original work except for quotations and citations which have been duly acknowledged. I also declare that it has not been previously or concurrently submitted for any other degree at UTAR or other institutions.

Name _____

Date _____

TABLE OF CONTENTS

LIST OF TABLES

LIST OF FIGURES

LIST OF SYMBOLS / ABBREVIATIONS

A_c	Free flow area, m^2
A_f	Total convective heat transfer area in contact with the fluid, m^2
A_s	Total heat transfer area, m^2
C_p	Specific heat capacity, $J.kg^{-1}.K^{-1}$
D_h	Hydraulic diameter, m
f	Friction factor
G	Mass flux of water based on minimum flow area, $\left(\frac{\dot{m}}{A_c}\right)$ $kg.m^{-2}s^{-1}$
$\bar{h}$	Convection heat transfer coefficient, $W.m^{-2}.K^{-1}$
L	Length of the heat sink
k	Thermal conductivity, $W.m^{-1}.K^{-1}$
$\dot{m}$	Mass flow rate of water, $kg.s^{-1}$
$\max x_0^i(k)$	Maximum value of $x_i^0(k)$ for the k^{th} response
$\min x_0^i(k)$	Minimum value of $x_i^0(k)$ for the k^{th} response
n	Number of simulation run
Nu	Nusselt number
p	Pressure, Pa
PD	Pressure drop
$\dot{Q}$	Amount of heat generated, W
$\dot{Q}_{conv}$	Amount of heat dissipated through convection, W
$\dot{Q}_{rad}$	Amount of heat dissipated through radiation, W
$\dot{Q}_{loss}$	Amount of heat loss due to poor insulation, W
Re	Reynolds number
r_h	Hydraulic radius, m
SP	Specific performance
$\bar{T}_s$	Average surface temperature, K
T	Temperature, K
TV	Temperature variation
u	Velocity, m/s
U_∞	Inlet velocity of water, $m.s^{-1}$
V	Volume of the heat sink, m^3
$\dot{V}$	Volumetric flow rate, m^3s^{-1}
V_f	Total fluid volume inside the heat sink, m^3
w_k	Normalized weight value of k^{th} performance characteristic
W_{pp}	Pumping power, W
$x_i^0(k)$	Normalized value of the k^{th} element in the i^{th} sequence.
$x_i(k)$	Value after the grey relational generation
$x_0^*(k)$	Referential sequence
$x_i^*(k)$	Comparative sequence
Y_i	Performance value of the simulation i^{th}
Δ_{min}	Smallest value of Δ_{0i}, 0
Δ_{max}	Largest value of Δ_{0i}, 1
Δp	Pressure drop through heat sink, Pa
$\Delta\theta$	Change of temperature, K
Δ_{0i}	deviation sequence between reference sequence and the comparable sequence with $x_0^*(k) = 1$

Greek symbol

η	Signal to noise ratio
ρ	Density, $kg.m^{-3}$
μ	Dynamic viscosity, $kg.m^{-1}.s^{-1}$
γ_i	Overall grey relational grade for i^{th} experiment
ψ	Distinguishing or identification coefficient

Subscripts

in	Inlet
max	Maximum
out	Outlet

CHAPTER 1

INTRODUCTION

1.1 General Introduction

Electronic components such as micro-processor, batteries and bipolar transistor have become an important part of modern life and it requires electricity to operate. When the electric current is passed through the electric component, it will generate heat due to ohm resistance. Uncontrollable increase of the heat generated will cause undesirable temperature rise and eventually lead to thermal runway. Based on International Technology Roadmap for Semiconductor (ITRS), the safest working condition for semiconductor devices must be kept under 85 ºC. With modern technology, the electronic component gradually became smaller in size which produces greater density power and generates heat flux as high as 100 $W.cm^{-2}$ that have been considered high for most electronic component nowadays. In most electronic component, conventional heat sinks are naturally used as thermal management media. However, the use of natural convection is proven not sufficient to dissipate a huge amount of heat generated. Insufficient cooling can cause the performance and life cycle of electronic component drop. Thus, high performance and cost-effective cooling solution are needed to solve the thermal management problem in modern electronic component.

Coolant such as air and liquid are generally used for the electronic component cooling. Liquid cooling has higher heat transfer coefficient compared to air cooling. Besides that, using liquid cooling also reducing the noise and can be used for smaller size the electronic component compare to air coolant which requires large spaces. Thus, it is shown that liquid cooling is more superior compared to air cooling. However, using liquid as cooling media in electronic component may have some drawbacks. Liquid cooling might not be cost-effective because of high cost and expensive component needed such as pump, heat exchanger and piping. Besides, it is more complex to install compared to air cooling and may have a leakage problem which will cause short circuit.

There are various types of heat sink used to dissipate heat generated from the electronic devices such as porous media, micro-channel heat sinks and spray cooling. One of the effective and efficient thermal management solutions is using micro-channel heat sink. Micro-channel heat sink is also considered as a small scale heat exchanger operates with fluid flows into the channel with a fraction of millimeter. Micro-channel heat sink has been proposed in 1980s by Tuckerman and Pease by changing the surface area to volume ratio to enhance single-phase heat transfer rate. Thus it will affect the convective in heat transfer thermal resistance. By changing the surface area to volume ratio, the smaller channel will produce better heat transfer coefficient compared to larger channel. Moreover, changing the width of the channel may exponentially affect the heat dissipation ability of the micro-channel heat ink as well as pumping power. Therefore, the design of micro-channel heat sink is

important to derive optimum cooling performance and minimum pumping power.

Although there are much research conducted to find the best possible design and technology to realize the full potential of micro-channel heat sinks for modern electronic devices, the research still inadequate and not fully optimize the design of micro-channel heat sinks, especially for high heat flux application. The problems associated with a conventional straight channel are thermal boundary development, high-pressure drop and large variation of temperature. Thus, the focus of this study is to design and develop novel micro-channel heat sinks and examines their thermal performance in the high heat flux application.

1.2 Importance of Study

This study is related to the common problem that usually occurs in electronic components nowadays which is a huge amount of heat being generated. When the electronic component generated too much heat, the functionality and reliability might be at risk. Thus, effective thermal management is important to ensure electronic components perform smoothly and reliably. Besides that, when the electronic component is subjected to uneven cooling, hot spot might be produced inside the electronic component. This phenomenon will affect the performance and shorten the life cycle of the electronic component. Therefore, micro-channel heat sinks need to be designed properly to ensure the heat generated is dissipated effectively to

avoid any hot spot occurs in the electronic components. Furthermore, most of the electronic component has optimum operating temperature in the range of 70 ºC to 80 ºC. When exceeding the optimum range, the electronic component might not perform smoothly and decrease its reliability. The heat controlling method using micro-channel heat sink can dissipate the heat generated effectively and prolong the cycle life of the electronic component.

1.3 Problem Statement

The function of the micro-channel heat sink is to dissipate the heat generated in the electronic component. By changing the surface area to volume ratio can manipulate the heat dissipation rate of the micro-channel. Straight channel is commonly used as a heat sink in the thermal management of electronic devices.

However, the cooling efficiency of the straight channel is decreased along the flow direction and lead to large variation of temperature from the downstream to upstream. Besides, continuous development of the thermal boundary layer along the channel will increase the variation of temperature from upstream to downstream. Therefore, the micro-channel heat sink design needs to study to overcome this problem such as minimizing the thermal boundary layer development and maintain the coolant cooling capacity along the flow direction.

1.4 Aim and Objectives

The aim of this study is to design and develop the micro-channel heat sink for high heat flux application. The specific objectives of this study as follows:

1. To design the micro-channel heat sink for high heat flux application
2. To optimize the design of micro-channel heat sink numerically
3. To evaluate the performance of micro-channel heat sinks experimentally
4. To validate the simulation results with experimental works

1.5 Scope and Limitation of Research work

In this research work, the priority focus is to design and develop of a novel micro-channel heat sink which can dissipate heat flux in high heat flux as high as 100 $W.cm^{-2}$. Theoretically, by increasing the surface area to volume ratio of the micro-channel heat sink, the thermal performance can be increased as well. Therefore, the scope of study is to develop a new type of micro-channel to improve the thermal performance of the conventional micro-channel to suit for high heat flux application. A CAD model is created to optimize the heat transfer performance based on the design parameter which is the fin length, width, transverse distance, channel size, and number of segmented zones. The micro-channel heat sink for this research work is

targeted to dissipate 800 W of heat load in the footprint of 30 × 30 mm using minimum amount of flow rate from 5 gs^{-1} and average temperature and variation below 5 ºC.

Although the thermal performance of the new micro-channel heat sink design may exceed the performance of the straight channel heat sink, complex shape of the new micro-channel design may affect the pressure drop across the micro-channel heat sink thus affecting the power consumption. Therefore, Taguchi-Grey optimization technique is used to optimize the micro-channel design to achieve a balance in thermal performance, variation of temperature and pumping power.

1.6 Contribution of Research Work

In this research work, the new design of micro-channel heat sink is developed to cater for thermal management solution for nowadays and future electronics devices. The new design of the micro-channel heat sink is divided into three segmented with vary fin total surface area to volume ratio of fin. The novel micro-channel will disrupt the thermal boundary layer development and enhanced fluid mixing along the flow path. Cooling capacity of the coolant can be improved through the varying fin total surface area to volume ratio along the flow path. The new design of the micro-channel heat sink is able to cool the chip with the heat flux of 800 W to 56.6 ºC, pumping power of 0.13 W using 15 gs^{-1} with variation of temperature less than 5 ºC.

1.7 Research Work Outline

The thesis is organized as follows, chapter two describes different geometric design of the micro-channel such as straight channel, wavy channel, pin-fin, fan-shaped ribs, dimples, oblique fin, and common cooling fluids used. Chapter three describes the methodology of this work from the modeling process then numerical analysis step and lastly describes the experimental setup for this work. Chapter four discusses the numerical simulation results of the micro-channel heat sink and experimental results. Chapter five compares the numerical and experimental result. Finally, chapter six summarizes the findings in the research work and highlight future work.

CHAPTER 2

LITERATURE REVIEW

2.1 Introduction

Thermal management plays a significant role in many engineering applications especially in the design of electronic devices. Advancement of electronic technology has led to stringent thermal management requirement to match the electronic devices power density. Hence, heat transfer at the micro-scale level has gained astounding demands and opportunities for thermal management system research and development. Moreover, advancement in the modern microelectronics industry and followed by the trend of increasing packaging density, acceptable heat removal target could be reached to 10000 $W.cm^{-2}$ and surface temperature must be less than 100 ºC for nanometer size of the chip in the regular microelectronic devices (Khan et al. 2014). Furthermore, demand for cost-effective cooling solution has been increasing due to market demand for cheaper electronic devices. In 2012, International Technology Roadmap for Semiconductor (ITRS) indicated that in 2020, integrated circuit (ICs) power density will increase up to 1000 $W.cm^{-2}$. This further indicates that traditional cooling solution cannot cope with high heat flux generated by the IC chips. Furthermore, ITRS also highlighted that optimum junction temperature for semiconductor is about 85 ºC (Prajapati et al. 2016). Number of transistors per unit area continued to increase in the past

five decades and this trend is expected to progress affirmed by Moore's Law. Later production of electronic chips is likely to develop about 5000 $W.cm^{-2}$ of background heat fluxes and there will be more than 10000 $W.cm^{-2}$ at hot spots. This has become a real challenge to remove heat generated from the ICs (Brinda et al. 2012, Abdoli et al. 2015). Therefore, heat generation problem needs to be solved urgently to ensure smooth operating of the device and growth of the electronics industry. In order to maximize the device performance and cycle life, the device must be configured with an optimum cooling solution. Besides, characteristic length of the cooling devices needs to be reduced to improve compactness of the system. Hence, micro-channel heat sink is the most favorable cooling solution for high-power density devices. Micro-channel heat sinks have found its applications in real life applications such as military and defense, bio-engineering, medical, nuclear industry, solar cell, fuel cell, and electronic industry. There are many factors influence the micro-channel heat transfer performance such as channel geometry design, rarefaction, surface roughness, fluid viscosity, electrostatic effect, channel wall axial heat conduction, shape factor, etc. These factors must be taken into account in the micro-channel heat sinks design.

1980s, Tuckerman and Pease compared the performance of the micro-channel heat sink with conventional or macro-channel heat sink. In the single-phase fluid flow, heat transfer rate is significantly enhanced by using micro-channel heat sink. High heat transfer performance exhibited from the micro-channel heat sinks is contributed by expanding the overall heat transfer area to volume ratio (Khan et al. 2014, Prajapati et al. 2016). Therefore, micro-

channel heat sink has an advantage in the thermal management due to smaller geometry size and low coolant flow requirements. Heat transfer of the micro-channel takes place either toward or away from the separating wall in a transient manner. Two crucial occurrences associated with the heat transfer in the micro-channel are cooling fluid flow and channel walls heat transfer. For a single-phase liquid cooling, up to 7900 $W.cm^{-2}$ of heat flux and 0.09 $K.W^{-1}$ of thermal resistances can be dissipated easily through the micro-channel heat sink (Rubio-Jimenez et al. 2016). However, heat transfer performance of the micro-channel in the single-phase convective is subjected to cost, pressure drop across the micro-channel and development of large temperature gradient on the flow path as well as amount of heat dissipated was limited by the choice of coolant used. Moreover, non-uniformities in temperature distribution will cause hotspots and reduce the efficiency and reliability of the electronic devices

Thermal conductivity of the cooling fluid can be improved by adding metallic fine suspended particles into the base fluid. Heat transfer performance using nanofluids is more effective than pure coolants. This is due to nanofluids have higher thermal conductivity to transfer the heat out of the devices (Joshi et al. 2014). However, there are negative effects associated with nanofluids such as drastic pressure drop, fouling, clogging, sedimentation and erosion that will harm the cooling system. However, recent development of the nanotechnology made it possible to produce a smooth plate channel that can overcome this problem (Chen and Ding. 2011). Thermal and hydrodynamic boundary was interrupted periodically by a smooth plate channel which

promotes better mixing at different temperatures of fluid parcel (Ebrahimi et al. 2015). In addition, flow boiling with micro-channel heat sinks has shown a great potential for high heat flux application. However, growth of the bubble will cause flow reversal, oscillation of fluid flow, oscillating of system pressure and slip phenomenon at the micro-channel wall will cause the flow field not fully developed (Khan et al. 2014). Therefore, it is important to investigate the factors affect the heat transfer mechanism in the micro-channel heat sink (Xia et al. 2014).

2.2 Geometrical Design

Geometrical design of the micro-channel is crucial to understand the mechanism of the heat transfer enhancement. Researchers have discovered that mechanisms of heat transfer can be improved through thinning of the thermal boundary layer, fluid mixing and increase fluid flow velocity gradient on the heated surface (Zhai et al. 2015). Increasing pumping power, small channel width-to-depth ratio and the large channel fin width-to-depth ratio were observed for the heat transfer enhancement in the micro-channel heat sink (Fan et al. 2014). Micro-channel with ribs, grooves, cavities, and complex structure have become one of the potential solutions for heat transfer enhancement (Fan et al. 2014, Chiu et al. 2014).

2.2.1 Straight channel

Wang and Peng examined the performance of forced convection heat transfer of deionized water and methanol through a rectangular micro-channel heat sink. Effects of different micro-channel width, distance between two micro-channel walls and different cooling fluids are being investigated (Wang and Peng. 1994). Stainless steel plate with width of 18 mm, length of 125 mm and height of 0.7 mm with micro-channel width ranging from 0.2 mm to 0.8 mm was designed in this study. Experimental results indicated that the heat transfer coefficient increment was subdued as width of the micro-channel decreased. Flow phenomenon in the micro-channel is defined by the Reynolds number. The Reynolds number is a dimensionless quantity to predict the fluid flow situation and transition of flow from laminar to turbulent flow. The Reynolds number is defined as

$$Re = \frac{\rho u L}{\mu} \qquad (2\text{-}1)$$

Fully developed heat transfer regime in the straight channel is started at Reynolds number of 1000-1500 and transition of laminar to turbulent flow in the micro-channel is affected by fluid temperature, velocity, and size of micro-channel.

Peng and Peterson have further the work of Wang and Peng (Wang and Peng. 1994) in examining the fluid flow characteristic and heat transfer of the rectangular micro-channel heat sinks (Peng and Peterson. 1995). They

discovered that temperature and velocity of the cooling fluid have heavy influence on the heat transfer and micro-channel wall temperature. Thus, heat transfer coefficient in the laminar and transition flow regimes is affected by varying the cooling fluid temperature, cooling fluid velocity and micro-channel size. This further evidence that the Reynolds number is not an only factor to determine the heat transfer characteristic in the micro-channel heat sink. Rahman investigated the heat transfer performance and friction factor of two different micro-channel configurations which are known as parallel pattern (I-type) consists of 12 channels and serial pattern (U-type) (Rahman. 2000). Silicon 100 wafer was used to fabricate the micro-channel and microelectronics. I–channel resulted in a smaller pressure drop while the flow rate in each channel in the U-channel is large. The channel width is set to 1 mm and a spacing of 2 mm was used to construct the micro-channel. The experimental analysis concluded that U-channel has higher heat transfer performance due to the total length of the channel is three times higher than the I-channel.

Siva et al. studied the influence of flow structure and hydraulic diameter/area channel ratio under different Reynolds number for parallel or straight micro-channel (Siva et al. 2014). The micro-channel dimension is 0.088 mm, 0.176 mm, and 0.352 mm with a fixed number of channel and channel widths. The result indicated that higher pressure drop will induce more uniform flow distribution and reduce the surface temperature of the chip. Variation of temperature at the chip surface with 0.352 mm and 0.176 mm channel widths are 5 ^{o}C and 3.5 ^{o}C, respectively. High surface area to volume

ratio of the parallel micro-channel will produce high heat dissipation rates and it is a good candidate for the cooling system. However, the efficiency of the parallel micro-channel heat sinks can be reduced by non-uniform flow distribution across the micro-channel heat sink which is known as flow mal-distribution. This will cause the formation of localized hot spots in the devices. High amplitude and low-frequency oscillation attributed to the presence of flow reversal is the main cause of flow mal-distribution. Siva et al. observed that pressure drop in the channel width of 0.088 mm is higher than the channel width of 0.176 mm. Reduction of channel width will cause 3 ^{o}C improvements in the temperature variation on the surface (Siva et al. 2014, He et al. 2016). This showed that changing of channel size caused the difference in flow distribution and affects the heat transfer performance in the micro-channel. Straight micro-channel heat sinks design is illustrated in Fig 2.1.

Raghuraman et al. used copper to fabricate the micro-channel heat sink with the width of 0.036 m, length of 0.031 m, and consists of 122 numbers of channels. The width of the wall is 0.150 mm with a height of 7 mm (Raghuraman et al. 2016). Different aspect ratio has been fabricated which is 20.00, 30.00, and 46.66 corresponded to the height of 3 mm, 4.5 mm and 7 mm, respectively. The channel width was kept constant at 0.015 mm. It is found that the pressure drop is the highest for the aspect ratio of 20 compared to 30 and 46.66, which is caused by different mass flow rate shifted along the micro-channel pathway. Hence, the large aspect ratio will produce a large variation of outlet temperature. From the numerical analysis, the aspect ratio of 30 is the preferred choice and amount of heat removal is at an optimum

level. Although straight micro-channel is commonly used for cooling system design, the cooling efficiency is decreased along the flow direction causing a large temperature difference between inlet and outlet. This is the main reason to attract and encourage more researchers to improve the heat removal capabilities of the micro-channel heat sink.

Chai et al. investigated the flow characteristic in the micro-channel by introducing the staggered rectangular geometry in the micro-channel to improve the fluid mixing (Chai et al. 2016). They used different configurations of rib inside the micro-channel heat sink to interrupt the fluid flow which causes a change in the pressure drop and heat transfer. There are five different shapes of offset ribs such as rectangular, isosceles triangular, backward triangular, forward triangular and semi-circular to interrupt the boundary layer development in the micro-channel (Chai et al. 2015). Simulation results showed that at Reynolds number less than 350, micro-channel heat sink installed with forwarding triangular ribs gave the highest thermal performance. On the other hand, at Reynolds number larger than 400, semi-circular offset ribs gave the highest thermal performance. Chia et al. also studied the effect of thermal resistance and pumping power on the thermal performance of the micro-channel under laminar flow (Chai, Xia and Wang. 2016). The study showed that when the fluid flow had been interrupted by the introduction of the ribs, it will improve the heat transfer coefficient. The velocity distribution has changed with the presence of the offset rib compared to the smooth channel. Interruption of boundary layer formation, recirculation or re-creation of the secondary flow was the most noticeable characteristics. Chia et al. also

stated that the installation of the rib and the influence of rib's height improve the performance of micro-channel heat sink (Chai et al. 2016, Chai et al. 2015, Chai, Xia and Wang. 2016).

Li et al. introduced vertical Y-shaped bifurcation plates to improve the performance of the straight micro-channel heat sinks (Li et al. 2014). There are four different configurations of the Y-shaped bifurcation plates with different 'Y' angle. It is found that the thermal resistance of the micro-channel installed with Y-shaped bifurcation plates decreased as the inlet velocity increased. At the flow velocity of 1.4 ms^{-1}, the thermal resistance of the new micro-channel is decreased to about 3/5 compared to straight micro-channel. The optimum configuration of the Y-shaped bifurcation plates is with Y angle of 90^{o}. However, the disadvantage of the current design is the high-pressure drop throughout the micro-channel.

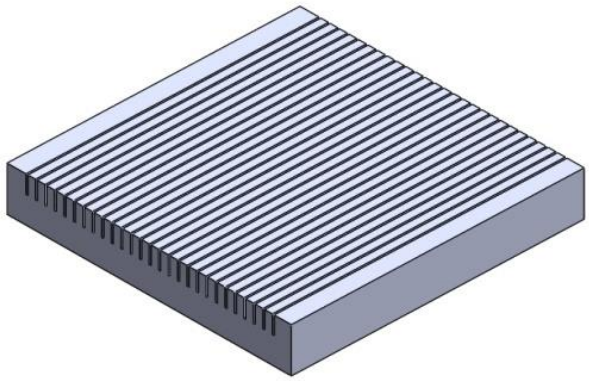

Fig. 2.1 General design for straight micro-channel heat sinks

(Naqiuddin et al. 2018)

2.2.2 Wavy channel

Adaptation of wavy wall has been applied commercially in 1980s on the vehicles and transpiration re-entry cooling of rocket booster, ablative surfaces cross-hatching and combustion chambers film vaporization (Vajravelu and Sastri. 1980). Besides, it can also be applied to the electronic devices to dissipate the heat generated. Thus, another micro-channel heat sink design is wavy channel design as illustrated in Fig. 2.2(a). Wavy design can induce a Dean's vortices and alternating secondary branch which help in fluid mixing inside the channel as shown in Fig. 2.2(b). Dean's vortices occurred when the flow in the wavy channel is very high and the flow is unstable and secondary flows are developed which introduce pairs of streamwise-oriented vortices. Dean number is used to characterize the dean vortex flow can define in Eq. 2-2.

$$De = Re\left(\frac{d}{r_i}\right)^{1/2} \tag{2-2}$$

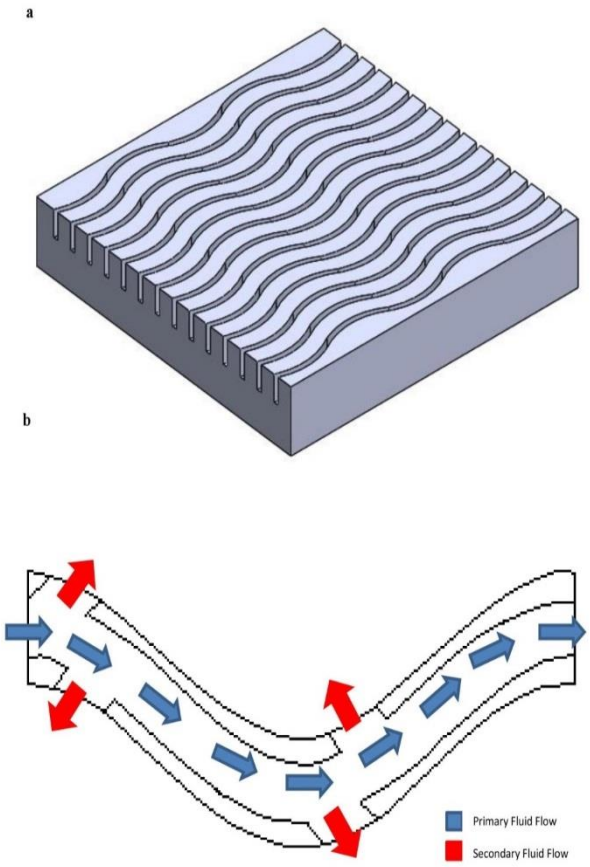

Fig. 2.2(a) Wavy design micro-channel heat sinks (b) alternating secondary branch which help in fluid mixing inside the channel (Naqiuddin et al. 2018)

Vajravelu and Sastri examined free convective heat transfer between the wavy channels and parallel flat wall through systematic analysis. The study showed that waviness of the wall affected the flow and heat transfer performance (Vajravelu and Sastri. 1980). Wavy pattern enhanced heat transfer coefficient as waviness is increased. However, there was a limitation on other parameters such as maximum wavelength or waviness allowed before the heat transfer performance deteriorates.

Habib et al. conducted a numerical analysis of the converging and diverging channel. The channel height is 1.16 mm and width of 5.08 mm with seven continuous corrugates vary in a sinusoidal mode. Two different aspect ratios of 0.27 and 0.34 are used in the numerical study (Habib et al. 1998). Habib et al. indicated that as the aspect ratio is increased, 15 % increment of the local heat transfer is recorded due to the separation reduction when the swirl number is increased.

Chiam et al. studied the vortices that produced cross-channel mixing (Chiam et al. 2016). The experiment used a wavy channel with an amplitude of 0.15 and 0.075, respectively. The design will produce secondary flows which increase the pressure drop. However, secondary branches increased the performance of heat removal consistently along the fluid flow direction. Thus, wavy channels have great potential for high heat flux dissipation. Meanwhile, Mohammed et al. investigated various wavy micro-channel heat sink characteristics with the wavy channel amplitudes in the range of $0.125 \text{ mm} \leq \alpha \leq 0.5 \text{ mm}$ and Reynolds number in the range of $100 \leq Re \leq 1000$ (Mohammed et al. 2011). The temperature at the edge of the micro-channel heat sinks is high due to the non-reachable of cooling fluid. On the other hand, the cooling fluid is focused at the center of the heat sink. High heat transfer coefficient leads to a low-temperature region in the micro-channel heat sinks. The wavy channel will improve the fluid mixing inside the micro-channel heat sinks. In Mohammed et al. experimental works, the wavy channel with an amplitude of 0.25 was tested and discovered that high amplitude of the wavy channel will improve the heat transfer performance of the system. However, when the

amplitude of the wave increased further, the performance decreased as the poor mixing occurred. The study showed that the amplitude of 0.25 resulted in the highest temperature as compared to the straight micro-channel.

Rostami et al. examined the influence of the geometrical conjugate heat transfer using wavy micro-channel heat sinks (Rostami et al. 2015). Presence of recirculation flow in the wavy design helps in producing secondary circulation and improves the heat transfer. Increasing wall amplitude leads to heat transfer rate improvement. Sakanova et al. studied the heat transfer of the wavy micro-channel heat sinks from the three-dimensional aspect (Sakanova et al. 2014). Studies showed that thermal resistance was reduced when the high amplitude and short wavelength are used. Thinning of the thermal and hydrodynamic boundary layer showed a positive impact on the heat transfer rate. However, increasing the wavy amplitude will induce fewer wavelengths and causing the flow to be more vigorous. This action will introduce an additional pressure drop across the heat sink. Wavy design of the micro-channel has a high potential towards dissipating high heat flux. Heat transfer performance can be enhanced by varying the amplitude and wavelength.

Ma et al. characterized the thermal and fluid flow performance of the zigzag micro-channel heat sinks. They discovered that zigzag micro-channel heat sink can promote better temperature distribution. Decreasing the zigzag length to channel length ratio will increase the porosity and convection heat transfer area and thus lead to enhancement of the fluid flow turbulence

intensity (Ma et al. 2016).

2.2.3 Pin-fin

Research discovered that design of the pin fin micro-channel heat sinks as shown in Fig. 2.3 has better thermal performance compared to straight channel heat sinks. Some research has been done on the micro pin-fin. Shafeie et al. studied the thermal performance of the pin-fin micro-channel and pin fin heat sink as well as pumping power required through numerical simulation. The micro pin-fin length and width are about 1 mm and total heights vary from 0.5 mm to 1 mm (Shafeie et al. 2013). Pin–fin micro-channel with a depth of 0.5 mm gives the highest heat removal rate with low pumping power. For low pumping power, the heat removal performance of the pin fin heat sink is higher than that of the pin fin micro-channel and vice versa for high pumping power. Entropy generation minimization can be used to optimize the design of the heat sinks.

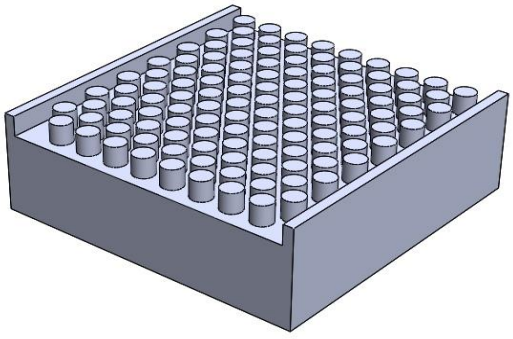

Fig. 2.3 Pin-fin micro-channel heat sink (Naqiuddin et al. 2018)

Zhai et al. used flow visualization technique-Micro PIV to analyze the formation of vortices caused by the ribs or cavities on the micro-channel heat sinks and experimental results are validated using Computational Fluid Dynamic (CFD) simulation (Zhai et al. 2016). The results showed that under small Reynolds number which is about 79.5, there are no vortices formed in the cavities zone. As the Reynolds number increased, the vortices form in the cavities intensifies the turbulent flow and enhances the heat transfer.

2.2.4 Ribs

Ghani et al. compared the performance of hybrid sinusoidal cavities and rectangular rib micro-channel heat sink using sinusoidal cavities micro-channel heat sink and rectangular rib micro-channel heat sink. Sinusoidal cavities of the micro-channel heat sinks are shown in Fig. 2.4. The geometric parameters focused in this study are relative cavity amplitude, relative rib width and relative rib length (Ghani et al. 2017). The used of cavities and rib in the micro-channel will enhance the thermal performance of the micro-channel compared to individual technique. The hybrid technique will reduce the pressure drop and eliminate stagnation zone present in the rectangular rib micro-channel. The hybrid technique will enhance fluid mixing by introducing chaotic advection. The heat transfer performance is proportional to the relative cavities, relative rib width, and relative rib length, while pressure drop exhibits an opposite trend. The optimum parameters of the hybrid micro-channel are relative cavity amplitude of 0.15, relative rib width of 0.3 and relative rib length of 0.5.

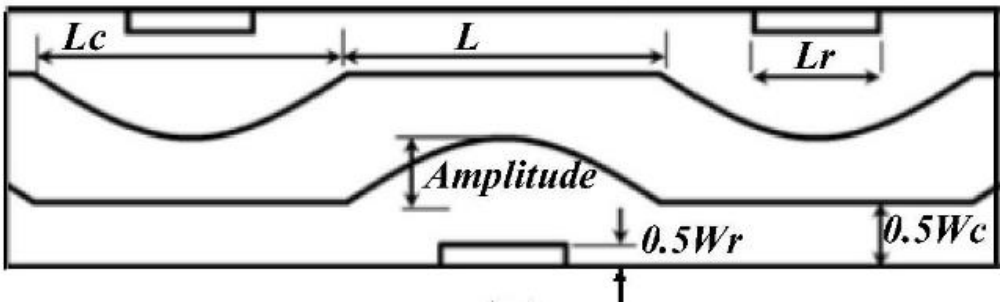

Fig. 2.4 Geometric design of sinusoidal cavities (Ghani et al. 2017)

Che et al. investigated dynamics thermal performance and the flow field of the droplet-based micro-channel. The influence of the channel cross-section aspect ratio, length of droplets and Peclet number are examined using steady-state numerical simulation (Che et al. 2016). It was found out that the thermal performance of the droplet-based is enhanced by the recirculating vortices and the gutter delayed the process of heat transfer. Besides, it also found that in the slug region between droplets can improve the heat transfer by transporting the hot fluid to the center of the droplet and pushing away fresh fluid to the wall (Che et al. 2016). Vary the flow passage cross-section give advantages in the heat transfer process by interrupting the thermal boundary layer development and increase the effective heat transfer area. However, the pressure drop across the micro-channel is also increased as the flow disturbance improved. Reducing the flow velocity can be done by increasing the aspect ratio of the micro-channel. Hence, the offset zigzag droplet is proposed.

Li et al. studied the geometric parameters effects of the micro-channel heat sink with triangular cavities and rectangular ribs. Besides, the effects on heat transfer performance and pressure drop are also being investigated. It is found that triangular cavities intensified the mainstream disturbance, enhanced the fluid mixing and interrupt the thermal boundary layer development (Li et al. 2016).

Wang et al. investigated the effect of different cross-section area such as rectangular, triangular and trapezoidal on the heat transfer performance and flow characteristics of the micro-channel heat sinks (Wang et al. 2016). The combination of either cavities or ribs can help in improving the heat transfer due to flow disturbance. This showed that heat transfer can be enhanced by creating flow disturbance. This will create the cooling fluid flow characteristic which has a higher heat transfer coefficient and help in dissipating the heat generated in the electronic devices.

2.2.5 Dimples

Xu et al. investigated the effectiveness of dimples in enhancing the cooling performance (Xu et al. 2016). Dimple micro-channel heat sink is shown in Fig. 2.5. The flow is laminar with a Reynolds number of 500 and the heat transfer performance is numerically investigated. The research found out that convection heat transfer under laminar flow is enhanced by the transverse convection caused by the dimple effect and the pressure drop is not significant.

Introduction of a dimple in micro-channel effect the heat transfer only due to the flow behavior and pressure drop difference between both conventional micro-channel and micro-channel with dimples is not very different, therefore, the pressure drop is considered not significant. Hence, another factor in micro-channel design can be considered.

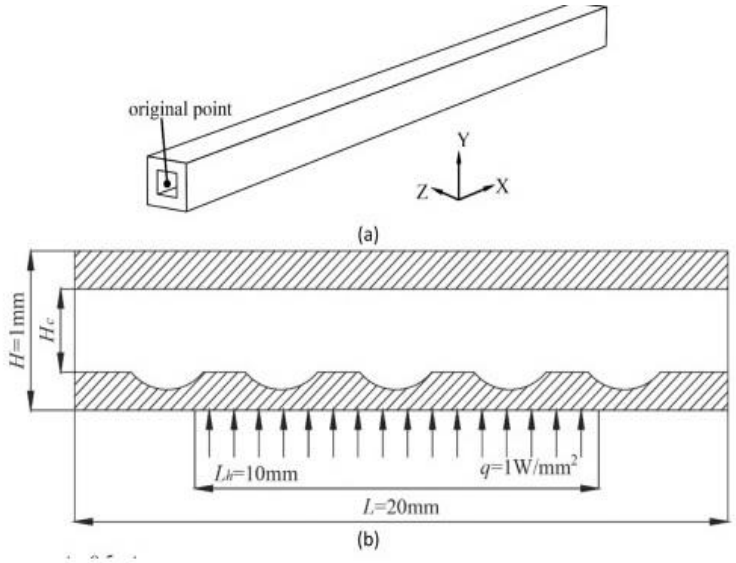

Fig. 2.5(a) 3D model geometric design with dimple (b) cross-sectional view (Xu et al. 2016)

2.2.6 Oblique fin channel

Oblique fin type of micro-channel is introduced to generate secondary flow and re-develop the thermal boundary layer in the micro-channel structure. Smaller channels were added at a certain angle between two main liquid channels to induce secondary flows which enhance the heat transfer without or with the addition of small pumping power. Through this method,

the enhancement factor of heat transfer is closed to 1.6 at Reynolds number of 300 compared to a conventional heat sink (Mou et al. 2016). Oblique fin is one of the augmentation techniques to improve heat transfer efficiency through fluid mixing (Lee et al. 2015). Fan et al. used numerical simulation and experimental works to examine the heat transfer performance of the cylindrical oblique fin and conventional straight channel as illustrated in Fig. 2.6. Based on the experiment, the velocity profile obstructs all entryway in the oblique fin causing re-initialization of the hydrodynamic boundary layer and significantly reduces the boundary layer thickness compared with a straight channel. Fluid flow velocity profile was upheld in the developing area throughout the oblique fin (Fan et al. 2013). Mou et al. and Lee et al. studied the effect of the secondary flow in the oblique fin. Lee et al. used 0.1 mm and 0.2 mm widths of the channel with the flow rate ranging from 100 x 10^{-3} L/min to 500 x 10^{-3} L/min. It was found out that oblique fin leads to a more uniform heat dissipation compared to the conventional straight channel (Mou et al. 2016, Lee et al. 2015). However, the edge effect can deteriorate the performance of the oblique fin micro-channel. Secondary flow generation and flow migration frequently occurred as the coolant travel downstream. This will cause flow mal-distribution and non-uniform temperature along the heat sinks footprint.

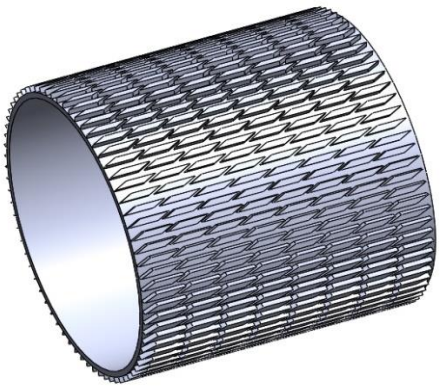

Fig. 2.6 Oblique fin micro-channel heat sink (Fan et al. 2013)

There are other micro-channel designs which help in the heat transfer enhancement. One of the designs is proposed by Colgan et al. which using silicon micro-channel as shown in Fig. 2.7 with staggered and continuous staggered fin. Staggered fin size is about 0.25 mm × 0.025 mm and flow channels width is 0.075 mm and depth is 0.195 mm (Colgan et al. 2007). Thermal performance of the micro-channel was observed and indicated that the difference between blunt and sharp-ended fins is not distinguished. The flow characteristic of different fins end did not affect the heat transfer performance due to secondary flow build up in each design disrupts the thermal boundary development and enhanced thermal performance. Appendix A summarized various designs of the micro-channel heat sinks for 100 $W.cm^{-2}$ heat flux and above.

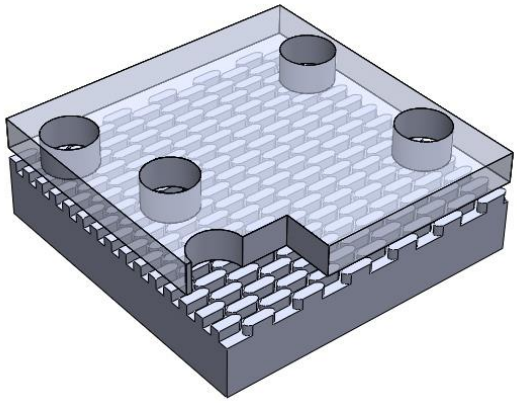

Fig. 2.7 Colgan design of micro-channel heat sink (Colgan et al. 2007)

2.3 Numerical and modeling simulation

Micro-channel design is very important to dissipate heat flux efficiently in electronic applications. There are many types of research on-going to determine optimum designs. However, thermal performance is depended on the design of the micro-channel. Therefore, numerical modeling is a useful tool to assess the performance of different micro-channel configurations. There are assumptions used in the numerical modeling such as the analysis is in steady state, fluid flow is incompressible, neglect the gravity effect and other forms of body forces, neglect the viscosity influence and dissipation effect, thermo-physical properties of the fluid and solid do not vary with temperature (Li et al. 2016). Numerical modeling is important in predicting the thermal performance and finding the optimal condition or configuration of the micro-channel heat sink.

Hung et al. created 3D CAD model with six different configurations of porous micro-channel heat sinks (porous-MCHS) which are outlet

enlargement, trapezoidal, rectangular, thin rectangular, sandwich distributions, and block to study the thermal performance and flow field (Hung et al. 2013). Trapezoidal and sandwich configurations produced more uniform temperature distribution which indicates that the heat flux can be transferred effectively via conduction from based surface to the heat sink. The pressure drop of the trapezoidal or sandwich distribution micro-channel is low. Incorporating of porous media in the micro-channel can effectively enhance the fluid mixing and redevelop the thermal boundary layer.

Priesnitz et al. investigated the effect of water and Cu-H_2O nanofluid in a swirl micro-channel heat sink (Priesnitz et al. 2016). Simulation results showed that the pressure drop of the micro-channel is depended on cavity height and inlet angle. Flow entrainment may adversely affect the thermal performance of the heat sink. In order for the swirl micro-channel heat sink use in high heat flux application, the fluid flow must be in the tangential direction to the inlet. Besides, the effect of nanofluid on the heat transfer enhancement is not significant as compared to a reduction of micro-channel height and inlet angle.

Xia et al. analysed the influence of different inlet and outlet manifold architecture (I, C and Z type), header shape (triangular, trapezoidal and rectangular) and micro-channel cross-section (rectangular, offset fan-shaped reentrant cavities and triangular reentrant cavities) on the flow field and thermal performance of the micro-channel heat sinks as shown in Fig. 2.8 (Xia et al. 2015). In this experiment, deionized water was used and 200 $W.cm^{-2}$ of

heat flux was assigned on the bottom of the heat sink. Experimental results showed that geometric shape effect on the micro-channel play an important role in affecting the heat transfer performance. The rectangular head shape seems to have better flow uniformity compared to trapezoidal and triangular configurations. Then, the optimized shaped of micro-channel is tested experimentally. Jetting and throttling mechanisms and addition flow disturbance near the wall introduced by offset fan-shaped reentrant cavities and triangular reentrant cavities can further enhance the heat transfer mechanism.

Xie et al. introduced Y-shaped bifurcations plates in the micro-channel to improve the performance of the rectangular micro-channel (Xie et al. 2015). Three different types of the micro-channel model with internal Y-shaped bifurcation with a dimension of 10 mm, 15 mm, and 25 mm were studied. Introduction of the Y-shaped bifurcations plate placed in the micro-channel will cause flow separation and vortex formation (Chingulpitak and Wongwises. 2015). Xie et al. also stated that Y-shaped can efficiently reduce the thermal resistance which is about 70% compared to conventional straight micro-channel.

Leng et al. investigated the performance of double layered micro-channel heat sinks using solid-fluid 3D conjugate heat transfer model (Leng et al. 2015). Different parameters have been tested to obtain the optimum heat sink performance such as channel number, channel width, bottom channel

height, and bottom coolant inlet velocity. These parameters are known to affect the thermal performance of the micro-channel heat sink. Fig. 2.9 illustrates the CAD model of the double-layered micro-channel heat sink. The optimal design is channel number = 54, channel width = 141 mm and inlet velocity of 0.99 ms^{-1} with a constant pumping power of 0.05 W.

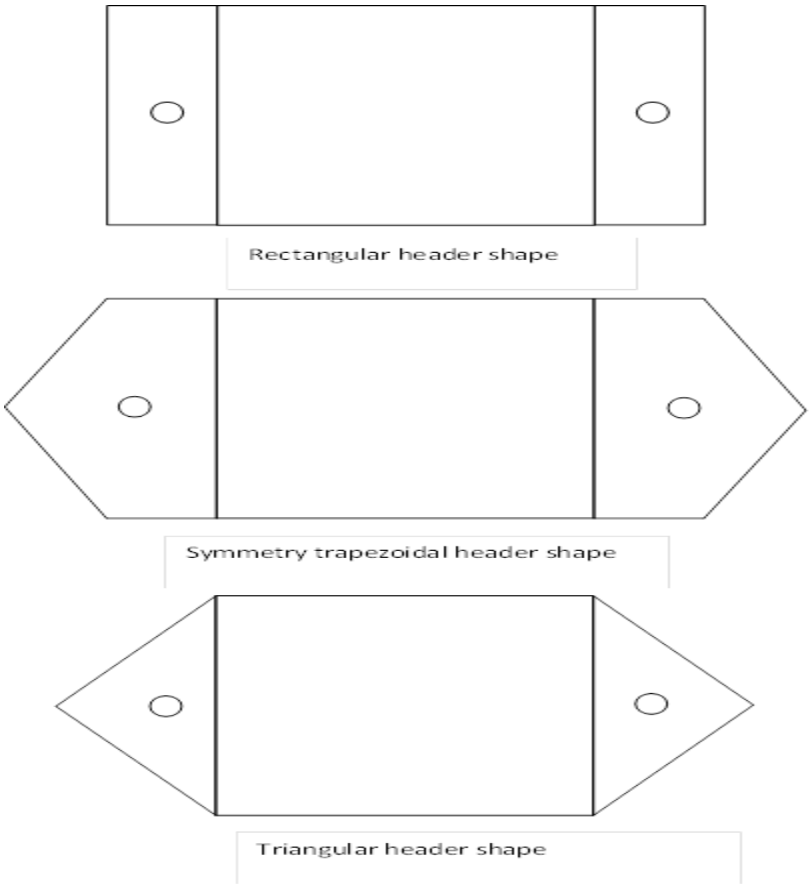

Fig 2.8 Schematic diagram of micro-channel heat sinks header design (Xia et al. 2015)

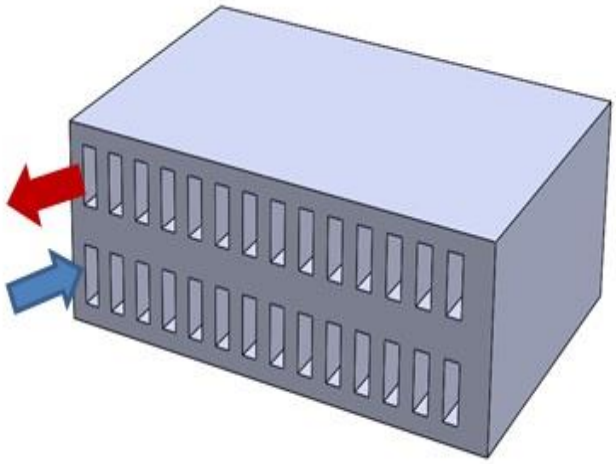

Fig 2.9 double layer micro-channel model (Leng et al. 2015)

Lin et al. believed that the optimal design of the micro-channel heat sink depended on the constraint conditions such as pumping power, the volumetric flow rate of the coolant and pressure drop (Lin et al. 2014). By raising the channel height, temperature uniformity at the bottom wall can be improved. By decreasing the channel length, thermal performance can also be improved due to the improvement of the temperature uniformity (Tran et al. 2016). Wong and Muezzin used a numerical approach to investigate the thermal performance of the parallel flow and counter flow configuration of the two-layered micro-channel heat sink. The effect of the micro-channel aspect ratio and middle rib thickness is also being investigated. It was found that small thickness of the middle rib is preferred to produce better thermal performance (Wong and Muezzin. 2013). The height and width of the micro-channel are about 0.8 mm and 0.2 mm, respectively. Numerical simulation results showed that for a channel width of 0.05 mm produced the highest thermal performance which can dissipate up to 7900 $W.cm^{-2}$ of heat generated.

Chuan et al. proposed a new concept of micro-channel design by replacing the solid fins with porous fins which reduced the pressure drop across the heat sinks (Chuan et al. 2015). The porous medium such as ceramics can decrease the thermal resistance of the micro-channel heat sinks. There are many types of research on the use of porous fin have been conducted. Although the thermal performance is improved, pressure drop and pumping power are high. Hence, porous fin micro-channel heat sink is a potential candidate to reduce the pressure drop. Presence of porous fins causing the non-zero velocity of coolant at the channel and porous fin interface which makes the coolant slip on the wall. Slip mechanisms help in reducing the drag effect which is one of the reasons for pressure drop reduction. Chuan et al. also indicated that around 43.0% to 47.9% reduction occurred compared to conventional micro-channel design.

Numerical investigations have been done by Wong and Lee. to predict the thermal and hydraulic performances of the micro-channel heat sinks with a different geometric parameter of the triangular rib (Wong and Lee. 2015). Rib width was varied to optimize the thermal performance. It was evident that by increasing the rib width and height, the heat transfer rate is also increased. The result from Wong and Lee. investigation showed that the optimum thermal enhancement of the micro-channel with triangular rib width of 0.1 mm, length of 0.4 mm, and height of 0.12 mm respectively. The thermal enhancement of around 43% can be achieved relative to non-interrupted rectangular micro-channel heat sinks. Based on Ahmed et al., the thermal performance can be

further improved by adding a cavity shape in the rectangular micro-channel (Ahmed et al. 2015). Yang et al. studied the rectangular rib-grooved channel and used numerical simulation to investigate the thermal performance. 18.2% of the increment in the thermal performance is found on the rectangular rib-grooved (Yang et al. 2015). Ribs inside the rectangular micro-channel can help in the thermal boundary redevelopment and enhanced the thermal performance of the micro-channel heat sinks. Wang et al. also conducted research on the ribs type of micro-channel. However, the friction factor is also increased due to the barrier effect of the ribs (Wang et al. 2015).

Cho et al. used the numerical modeling approach to investigate the fluid flow distribution in the micro-channel heat sink. Simulation results discovered that the flow distribution is depended on the design of the header. Then non-uniform heat flux effect on the different header design was examined and studied to optimize the header geometry (Cho et al. 2010). Different header design can influence the micro-channel heat transfer performance as discussed in the previous section. The header design used in the experiment is shown in Fig. 2.10 and the result showed that n = 4 is the most reasonable design to produce an optimum thermal performance.

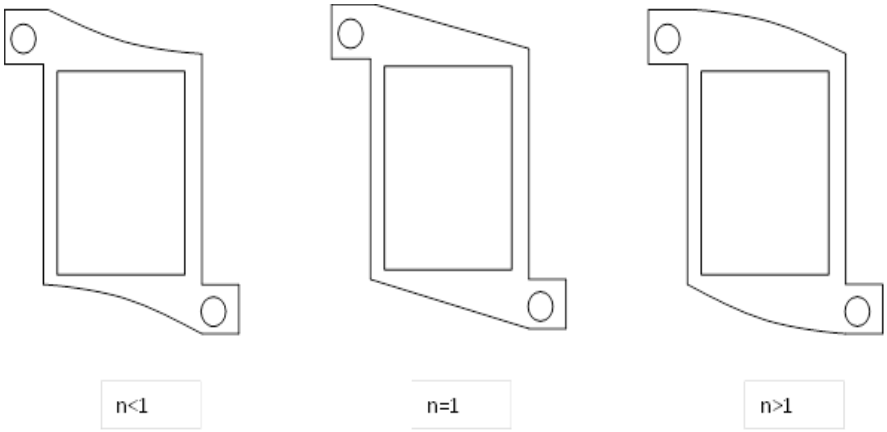

Fig 2.10 Example of header shape variation (Cho et al. 2010)

Micro-channel heat sinks were studied widely but the research on the micro-channel performance with the different channel such as circular, hexagonal, and rhombus is very rare (Alfaryjat et al. 2014). Thermal performance is affected by the type of channel and the aspect ratio. Thermal performance of the micro-channel heat sinks is increased when a smaller aspect ratio is used. Sakanova et al. studied the reduction in thermal resistance of the double layer and double side (sandwich structure) micro-channel heat sink. The simulation results show that a sandwich structure with counterflow showed a reduction of thermal resistance of 59%, 52%, and 53% compared to a single layer, double layer with the unidirectional flow and a double layer with counterflow, respectively (Sakanova et al. 2014).

Based on the literature above, numerical simulations are important to predict the optimal parameter and geometrical shape for better heat transfer performance in the micro-channel. Well distributed in the surface temperature and low thermal resistance are favorite for the micro-channel design (Alvarado

et al. 2010). Numerical and modeling simulation can be compared with the experimental work to validate the simulation results.

2.4 Two-phase flow boiling

In the semiconductor industry, thermal management using flow boiling in the micro-channel heat sinks is projected as one of the optimal solutions for high heat flux removal. In the two-phase flow boiling, a small amount of coolant flow is needed to maintain the uniformity of the wall temperature. Two-phase flow boiling can be achieved through modifying the channel structure into diverging, expanding, cross-link or re-entrant configurations. Among the configurations, the re-entrant configuration is well-known to induce the nucleation boiling which gives notable result led to a reduction of superheat in the wall and developed steady nucleation sites. Mitigation of two-phase flow instabilities is a good option for conventional rectangular, triangular or trapezoidal micro-channel heat sinks.

Two new solutions were introduced to suppress and delay the boiling instability inside the micro-channel heat sinks that can be easily employed. First is through surface morphology modification by changing the surface properties for suitable boiling performance enhancement. Second is through the introduction of the jet inside the micro-channel heat sinks that promoted fierce disruption in the channel flow stream and function as an effective way to disrupt the development of thermal and hydrodynamic boundary layers at channel wall (Khan et al. 2014). Micro-channel heat sinks performance is

associated with the solid material and coolant fluid properties as well as flow condition and geometric configuration of the channel (Hung et al. 2012). Nevertheless, removing the large heat fluxes is not sufficient by using air or fluids as the cooling medium. Heat flux that is above 1000 $W.cm^{-2}$ which is needed to be dissipated from the electronic component can be effectively removed through two-phase flow boiling (Riofrio et al. 2016).

Deng et al. studied the flow boiling performance of the re-entrant porous-based micro-channel heat sinks (Deng et al. 2015). Thermal performance, pressure drop, and two-phase flow instabilities were examined in this study by using ethanol coolant. Nucleate boiling is dominated at the re-entrant porous based micro-channel heat sinks at low heat fluxes. Mass fluxes and inlet sub-cooling are the factors that affect the heat transfer characteristic at moderate to high heat fluxes. As the magnitude of heat fluxes increased, the flow pattern changed from bubbly flow to slug flow, intermittent flow, annular flow and finally local dry-out. The pressure drop of the re-entrant porous micro-channel is proportional to the heat flux and vapor qualities at the saturated boiling region.

Yin et al. investigated the flow boiling of water using a large aspect ratio of micro-channel (Yin et al. 2017). A high speed camera was used to examine the thermal performance and pressure drop. When the critical heat flux is reached, the flow regime is preceded from discrete bubble flow to confined bubble flow then to sweeping flow and churn flow. Finally, the flow regime changed from churn flow to wispy flow. For a large aspect ratio of

micro-channel, the heat transfer process is dominated by nucleate boiling. Strengthening effect of the bubble confinement that occurred in a small aspects ratio yytii89809-0 of micro-channel does not occur in the large aspect ratio micro-channel. Heat transfer coefficient is the largest for sweeping flow and churns flow and pressure drop fluctuation did not occur in the wispy flow.

Deng et al. compared the two-phase flow boiling performance of the re-entrant micro-channel and conventional rectangular micro-channel with similar hydraulic diameter. Deionized water and ethanol were used as the coolant. The experimental results showed that the performance of the re-entrant micro-channel is outstanding at the moderate to high heat fluxes cases as compared to conventional rectangular micro-channel. Besides, the reduction of pressure drop and the mitigation of two-phase flow instabilities was achieved using re-entrant micro-channel (Deng, Wang et al. 2015).

Some research showed that as the vapor quality increase, the two-phase heat transfer coefficients decrease (Thiangtham et al. 2016). Vapor quality is an important factor influence the heat transfer coefficient. Vapor quality of about 0.55 is effective to reduce the heat flux. However, several drawbacks are associated with flow boiling such as a complicated structure which is difficult to manufacture in micro-scale and have a significantly large pressure drop in implementing a two-phase flow scheme. Moreover, the gas-liquid mixture is needed to flow into smaller scale micro-channel heat sink and became the main concern for the visualization and examines the heat transfer characteristic flow through micro-channel heat sinks.

2.5 Cooling fluid

Other than geometric design optimization, cooling fluids is another important factor affects the micro-channel heat transfer enhancement. There are many types of research focus on the direct contact of cooling fluid with the heat sink which involved heat transfer between fluids through a separating wall in a transient manner. Thus, a higher heat transfer coefficient can be achieved by improving the cooling fluids properties, which in turn enhanced the micro-channel heat sinks heat transfer performance. Most electronic applications are air cooled and the present data showed that air cooling contributed about 33% of the overall energy bill of the system. If the cooling system is replaced by liquid cooling, a significant reduction of energy consumption can be achieved. Liquid cooling with micro-channel heat sinks has been proved to be an effective and more favorable approach for high heat dissipation due to several advantages such as high cooling capacity, anti-seep, high integration, compactness, quiet operation, multiple pattern and ease of fabrication.

Water can be used as a cooling fluid due to its excellent thermal properties. Besides, the non-toxic nature of the water has an advantage for cooling applications (Jaikumar and Kandlikar. 2015). Sharma et al. have extensively studied the cooling of non-uniform multicore microprocessor power map by employing a static and energy preserving method to develop the micro-channel heat sinks. Fine and coarse channels are rationally distributed

over the hotspots and background respectively, while flow throttling zone is incorporated to distribute the flow in the different region of the chip. Simulation results showed that improvement of up to 57 % in chip temperature by using uniform embedded micro-channel and uniform flow distribution. Besides, about 30% improvement in chip temperature was achieved by using non-uniform embedded micro-channel and non-uniform flow distribution design (Sharma et al. 2015). Jaikumar and Kandlikar investigated the enhancement of boiling performance based on the hypothesis that micro-channel heat sinks have superior rewetting pathways and porous coating will provide additional nucleation sites (Jaikumar and Kandlikar. 2015). Separate liquid-vapor pathways were developed by the cohesive mechanism and promote suspension of critical heat flux by constantly feeding the nucleation sites with liquid. Thus, it has fulfilled the electronic application by satisfying the cooling requirement for the maximum allowable temperature of about 85 ^{o}C.

Mohammadian et al. investigated the effect of internal and external cooling of the Li-ion battery by passing electrolyte and water through micro-channel integrated with the battery. It is showed that internal cooling improved the temperature uniformity and also reduced the bulk temperature inside the battery. Internal cooling is more effective in reducing the deviation of the internal temperature 5 times higher than that of the external cooling (Mohammadian et al. 2015). Ethylene glycol is used to improve the freezing and boiling point of the water (Soltanimehr and Afrand. 2016, Sandhya et al. 2016). However, the thermal conductivity of ethylene glycol and water are

very low and result in poor convective heat transfer. However, by incorporating graphene nanoplatelets into the ethylene glycol and water to form a nanofluid can enhance the fluid thermal conductivity. It is found that about 21% and 16% increase in the thermal conductivity of ethylene glycol and water, respectively by loading about 0.5 vol % of graphene nanoplatelets into the fluid (Selvam et al. 2016).

Nanofluids are commonly used as an alternative to replace water or ethylene glycol-water mixture. One-step or two-step production is a common method used to produce nanofluids. Important elements for nanofluids production are nanoparticle material and base fluid. Various nanoparticles material has been utilized in the nanofluids such as oxide ceramic (Al_2O_3 and CuO), nitride ceramics (AlN and SiN), carbide ceramics (SiC and TiC), metals (Cu, Ag, and Au), semiconductors (TiO_2 and SiC), carbon nanotubes, and composite materials. These materials are commonly used together with a liquid base such as water, ethylene glycol, and oil (Ghale et al. 2016).

Liquid chemical method or physical vapor deposition (PVD) technique is one of the methods used to produce nanoparticles through a one-step process. Physical vapor deposition, however, did not receive the limelight due to the separation difficulty of the nanoparticles from the liquid. With recent development in nanofluids technology, a direct evaporation system has been developed whereby passing through a low vapor pressure flowing of liquid ethylene glycol. Copper vapor can condense into the nanoparticles which increase the thermal conductivity of the ethylene glycol to 40% by adding only

0.3% of the Copper nanoparticles concentration. However, this procedure can solely be used for low vapor pressure. The second method in producing nanoparticles is using chemical synthesis. This method can yield a steady Copper-in-ethylene glycol nanofluid. Under microwave radiation, Copper Sulphate Pentahydrate ($CuSO_4.5H_2O$) is reduced with Sodium Hypophosphite ($NaH_2PO.H_2O$) in ethylene glycol. This procedure is known for its simplicity and low-cost compared to PVD method.

Another method is a two-step process using the nanoparticles which have to produce first then blended with base fluids. This method is widely used in nanofluids production. The main reason is that nanopowders are easily available. However, agglomeration of the particles can occur particularly during the process such as drying, storage, and transportation due to the attraction force of Van der Walls since the preparation of nanoparticles and nanofluids is a separate process. Dried agglomerates nanoparticles form is mostly used which have bigger dimension compared to single particles. Sedimentation method is commonly used to determine the stability of the nanofluids. Comparison of engineered nanofluids with conventional solid-liquid suspension, engineered nanofluids possesses advantages in the intensification of heat transfer from its high surface area between the particles and fluids providing more heat transfer surface. Besides that, predominant Brownian motion of particles gives high dispersion stability and reduces the pumping power, particles clogging issues and easy to adjust the properties to suit the requirement. Those are the commonly known advantages of the nanofluids.

When discussing cooling fluid, thermal conductivity is one of the crucial parameters in improving the heat transfer performance. Compared with water or ethylene glycol, higher thermal conductivity is shown by nanoparticles, thus it can be an alternatives way for heat transfer and thermal conductivity improvement. The diameter of nanoparticles, volume fraction, viscosity, thermal conductivity and the temperature factor of the based liquid are the factors influence the thermal conductivity of nanofluids. From the literature, it is shown that the channel configuration and coolant type are the crucial factors to determine the heat transfer in the micro-channel heat sinks. In the 1990s, nanofluids as a new class medium of heat transfer were proposed by mixing solid particles with a diameter lower than 1×10^{-6} mm into the base liquid. Experimental result exhibited a dramatic improvement in the thermal conductivity and non-proportional relation between both nanofluids concentration and thermal conductivity.

Ghale et al. investigated the performance of the rectangular micro-channel heat sink with uniformly heated walls. CFD simulation is used to model the laminar forced convective heat transfer in the single and two phases flow with alumina/water nanofluids (Ghale et al. 2016). By dispersing the nanofluids in water, the ultrasonic bath is used to ensure the homogeneous dispersion of nanoparticles in the base fluids. Experiments results showed that nanofluids give excellent thermal stability and exhibit superiority over the pure water as the cooling fluid.

Liquid coolants which have high heat transfer coefficients is more preferable than the gaseous coolants to provide maximum heat transfer rate to the micro-channel heat sinks. However, commonly used liquid coolants such as water, oil, and ethylene glycol have a poor thermal conductivity compared to solid (Ahmed et al. 2016, Ebrahimi et al. 2016). The alternative way is to use nanofluids which showed a tremendous cooling capability due to its enhanced thermal conductivity compared to pure fluids. Hence, nanofluids have a great potential to enhance heat transfers (Ahmed et al. 2016). With the implementation of nanofluids, higher heat transfer coefficient at the entrance region is gradually decreased as the flow became fully developed. It shows the sensitivity of the nanofluids upon the thermal boundary development (Kuppusamy et al. 2013). Most of the research on the micro-channel heat sinks have been studied using conventional fluids such as water, ethylene glycol and mineral oil and it is very limited especially in trapezoidal grooves according to Kuppusamy et al. (Kuppusamy et al. 2013). The simulation results suggested that Al_2O_3 nanoparticles suspended in the water-based fluid provide the highest thermal performance in the trapezoidal grooved micro-channel heat sink. Peyghambarzadeh et al. compared the performance of the rectangular micro-channel heat sink using different concentrations of Al_2O_3 and CuO nanoparticles. Nanofluids such as Al_2O_3–H_2O and CuO–H_2O showed great improvement in the micro-channel heat sinks pressure drop and heat transfer compared with water. It is found that Al_2O_3 nanoparticles are less prone to deposition compared to CuO nanoparticles in water base fluid. Effects of nanofluids become less significant when the deposition of particles at a high

flow rate and high concentration of nanoparticles (Peyghambarzadeh et al. 2014).

The experiment conducted by Ahmed et al. studied the reduction of unwanted temperature deviation and also minimization of pressure drop in the double-layered micro-channel heat sinks. The focus is on rectangular and triangular double layered micro-channel heat sinks through modifying the structure and design. Nanofluids Al_2O_3-H_2O and SiO_2-H_2O with 4 x 10^{-7} mm in diameters of Al_2O_3 and SiO_2 in water base fluid are used. Percentage of nanoparticles used was 0.3%, 0.6%, and 0.9%, respectively. Nanofluids flow with Reynolds number ranging from 50 to 300 was used (Ahmed et al. 2016). The heat transfer coefficient increases with the inclusion of nanoparticle into the water base fluid. Therefore, heat dissipation performance is better than water alone. Pressure drop in the micro-channel is decreased as the flow distribution in the micro-channel became more uniform.

Radwan et al. investigated the performance of the micro-channel heat sink using two types of nanoparticles with different volume fraction for cooling process namely Aluminium Oxide (Al_2O_3) and Silicon Carbide (SiC) (Radwan et al. 2016). At a higher concentration ratio and lower Reynolds number, a large reduction of temperature can be achieved. Both types of nanofluids could contribute to the decreasing in temperature when the volume of the nanoparticles used is increased. SiC-H_2O performed better than the Al_2O_3-H_2O with high-temperature reduction. Wu et al. examined the effect of Al_2O_3–water nanofluids in enhancing the performance of micro-channel heat

sinks (Wu et al. 2016). When the inlet velocity is 2.5 ms^{-1}, about 8.0% reduction of thermal resistances is observed using Al_2O_3–H_2O nanofluids. This indicates that the presence of nanofluids in the micro-channel heat sinks can further reduce the thermal resistance leading to a better thermal performance. Compared with water, nanofluids can reduce the thermal resistance of micro-channel heat sinks and improved uniformity of temperature distribution with a difference of about 0.46 ºC only. Hence, a good thermo-physical property such as high thermal conductivity, high specific heat capacity, and less dynamic viscosity is important for nanofluids compared with other base fluids in the micro-channel cooling.

Comprehensive understanding of the nanofluids flowing through micro-channel heat sinks is necessary because of its feasible and effective in thermal management compared to conventional cooling fluids which can strengthen the convection heat transfer. Heat dissipation of micro-channel heat sinks mostly used nanofluids filled with Al_2O_3 and TiO_2 nanoparticles. Xia et al. compared the performance of micro-channel heat sinks with a traditional and optimized fan-shaped rib in the same dimension. The diameter of the nanoparticles is 5 x 10^{-6} mm owing to the high specific surface area and the active thermal motion (Xia et al. 2016). Increasing the volume fraction and the fraction resistance coefficient enhanced the thermal conductivity of nanofluids and dynamic viscosity. However, the thermal conductivity of nanofluids is decreased when the Reynolds number is increased. Yang et al. used numerical modeling to investigate the performance of CuO–H_2O nanofluids in the laminar and turbulent forced convection flow in the micro-channel heat sinks

(Yang et al. 2014). The simulation results showed that two-phase numerical models are more accurate to estimate the thermal resistance obtained through experimental works. The thermal resistance of the nanofluids in the laminar flow is smaller than water and inversely proportional to the particle volume fraction but proportional to the volumetric flow rate. Moreover, the pressure drop in the nanofluids cooled micro-channel is higher than that of the water-cooled micro-channel. Yue et al. compared the cooling performance of water-based nanofluids as the coolants in the micro-channel heat sinks through computational fluid dynamic simulation. In the numerical study, various inlet velocities and nanoparticles diameter were used as well as solution concentration (Yue et al. 2015). Based on the review, nanofluids is an alternative way of replacing traditional coolants such as water and ethylene glycol. The properties of nanofluids can be further investigated to improve the micro-channel heat sinks performance using new advancements in cooling technology in the future. The thermal conductivity of the nanofluids can be improved and used to dissipate high heat flux in the electronic devices.

2.6 Optimization

In order to increase the heat transfer and reduce the pressure drop in the micro-channel heat sink, several optimization techniques have been used to improve the heat sink designs (Ahmed et al. 2018). Sahin et al. have applied the Taguchi method to improve the convergence and divergence heat sink (Sahin et al. 2005). ANOVA is used to optimize the heat transfer and pressure drop characteristic of the heat sink by considering the contribution ratio of

individual design parameters. It is found that fin height, fluid velocity and the stream-wise distance between fins are the parameters affecting the heat transfer performance. On the other hand, the angle of attack is the most important parameter which causes the pressure drop in the heat sink. On the other hand, Chen et al. have optimized the efficiency of the thermoelectric generator using Taguchi method (Chen et al. 2015). The orthogonal array of L_{25} (5^6) with six design parameters namely external load resistance, hot side temperature, thickness and height of fins as well as length and width of the heat sink is used in the optimization process. It is found that the power output of the thermoelectric electric system has been successfully improved by 6 %. Moreover, the Taguchi method is also utilized to optimize the ground heat exchangers for cooling and heating applications (Pandey et al. 2017). The orthogonal array L_{27} (3^8) is used to optimize the minimum length required for a ground heat exchanger. The optimization results demonstrate that thermal conductivity and pipe diameter are the key parameters for improving heat transfer performance in the vertical and horizontal ground heat exchanger. Besides, Srikanth et al. have performed multi-objective geometric optimization to minimize the cooling time and maximize the heating time of the phase change material (PCM) based heat sink using a non sorting genetic algorithm (NSGA II) (Srikanth et al. 2015). The operation time of the PCM heat sink during the charging cycle can be stretched by 5 % via the optimization process and discharging cycle can be reduced by 12.5 %. Jang et al. have also optimized the heat transfer performance of the pin-fin radial heat sink using multi-objective optimization (Jang et al. 2014). The cooling performance of the pin-fin radial heat sink is successfully improved by 45 %

as compared to that of the plate-fin heat sink. Additionally, fin height is found to be an important factor that influences the cooling performance of the radial heat sink.

2.7 Summary

Hence, critical review of this topic will help understand the mechanism behind the heat flux dissipation and much-needed research in micro-channel heat sinks have to be continued and improved because of its great potential to be implemented in the near future. For future consideration, a better design can be implemented and tested based on the literature review. Micro-channel heat sinks design that adds secondary branch which promotes re-development of flow and thermal boundary can be used. However, the micro-channel pressure drop is crucial to be ignored, thus sharp edge design can be implemented to reduce the edge effect in micro-channel. As a conclusion, with the advancement of the technology nowadays, more micro-channel heat sinks in-depth study can be done to overcome the high heat flux demand in the electronic devices. From the critical review, for this research work, a novel micro-channel heat sink can be designed using the sharp edge to improve the heat transfer performance by re-development of the thermal boundary from secondary flow inside the micro-channel heat sink.

CHAPTER 3

RESEARCH METHODOLOGY

3.1 Introduction

In this chapter, the methodology for this research work is discussed in details. In the first section, numerical modeling procedure of the micro-channel heat sink design is explained. This also included the design of experiment using Taguchi method and also optimizing the design using Taguchi-Grey method with consideration of specific performance, a variation of temperature and pressure drop. Lastly, experimental work for the current study is also discussed.

3.2 Micro-channel heat sink design

There are two different types of micro-channel heat sink used in the current study namely straight-channel and segmented micro-channel heat sink. The CAD model of the heat sinks is developed using Solidworks 2016. Next, commercial computational fluid dynamics software, namely ANSYS CFX is employed to examine the heat transfer and flow characteristics in the micro-channel heat sinks. The size of the micro-channel heat sinks is 3 mm (width) x 3 mm (length) x 5 mm (height), whereas the flow channel of the straight-channel heat sink is 1 mm (width) x 2 mm (depth). Six design parameters are

applied to optimize the segmented micro-channel heat sink including fin width, fin length, fin transverse distance, number of segments, channel width and mass flow rate. The designs of the straight-channel and segmented micro-channel heat sinks are depicted in Fig. 3.1.

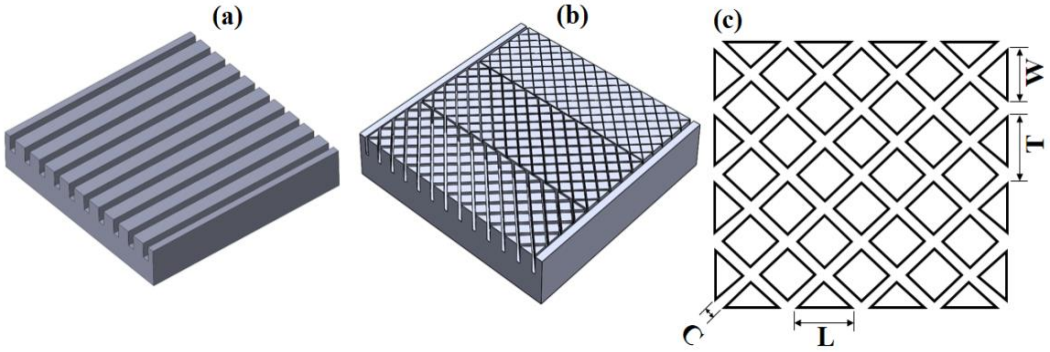

Fig. 3.1 Design of straight and segmented micro-channel heat sink

3.3 Computational fluid dynamic analysis

In this section, a three-dimensional conjugate heat transfer model is used to investigate the flow field and thermal performance of the micro-channel heat sinks. Several assumptions are made in this simulation: (a) constant thermophysical properties, (b) no energy source present in the fluid, (c) steady state flow condition, (d) incompressible flow, (e) no gravity effect and (f) the micro-channel is well insulated with no heat loss. In order to solve the conjugate heat transfer problem, continuity, momentum and energy equations as following are used (Ansys. 2010, Saw et al. 2016, Saw et al. 2017).

Continuity equation:

$$\frac{\partial u_x}{\partial x} + \frac{\partial u_y}{\partial y} + \frac{\partial u_z}{\partial z} = 0 \quad (3\text{-}1)$$

X-momentum equation:

$$\rho\left(u_x \frac{\partial u_x}{\partial x} + u_y \frac{\partial u_x}{\partial y} + u_z \frac{\partial u_x}{\partial z}\right) = -\frac{\partial p}{\partial x} + \mu.\left(\frac{\partial^2 u_x}{\partial x^2} + \frac{\partial^2 u_x}{\partial y^2} + \frac{\partial^2 u_x}{\partial z^2}\right) \quad (3\text{-}2)$$

Y-momentum equation:

$$\rho\left(u_x \frac{\partial u_y}{\partial x} + u_y \frac{\partial u_y}{\partial y} + u_z \frac{\partial u_y}{\partial z}\right) = -\frac{\partial p}{\partial y} + \mu.\left(\frac{\partial^2 u_y}{\partial x^2} + \frac{\partial^2 u_y}{\partial y^2} + \frac{\partial^2 u_y}{\partial z^2}\right) \quad (3\text{-}3)$$

Z-momentum equation:

$$\rho\left(u_x \frac{\partial u_z}{\partial x} + u_y \frac{\partial u_z}{\partial y} + u_z \frac{\partial u_z}{\partial z}\right) = -\frac{\partial p}{\partial z} + \mu.\left(\frac{\partial^2 u_z}{\partial x^2} + \frac{\partial^2 u_z}{\partial y^2} + \frac{\partial^2 u_z}{\partial z^2}\right) \quad (3\text{-}4)$$

According to the first law of thermodynamics, amount of heat rate added to the fluid domain and also the work is done is equal to the energy changed in the fluid domain (Ansys. 2010, Saw et al. 2016, Saw et al. 2017). Thus, the energy equation can be described as in Eq. 3-5:

Energy equation:

$$\rho c_f\left(u_x \frac{\partial T}{\partial x} + u_y \frac{\partial T}{\partial y} + u_z \frac{\partial T}{\partial z}\right) = k_f.\left(\frac{\partial^2 T}{\partial x^2} + \frac{\partial^2 T}{\partial y^2} + \frac{\partial^2 T}{\partial z^2}\right) \quad (3\text{-}5)$$

Where ρ is the density of the fluid, u is the mean velocity, T is the temperature, k is the thermal conductivity of the fluid, p is the pressure of the fluid and μ is the viscosity of the fluid.

In order to appropriately apply the turbulence model in the CFD analysis, it is necessary to ensure that the flow is turbulent based on the computed Reynolds number (Re). In this study, the Reynolds number ranges

from 3370 to 11236 for straight-channel heat sink and ranges from 260 to 2080 for a segmented micro-channel heat sink. According to Fan et al., the flow regimes in the segmented micro-channel heat sink or straight-channel heat sink are unstable and chaotic. A proper turbulence model is needed to accurately predict heat transfer simulations (Fan et al. 2014). In addition, it is noted that no single turbulence model is accepted universally for all classes of industrial application and the results have not been verified and validated (Wu et al. 2010). The turbulence model only yields accurate predictions in wall-bounded flows or free-shear flows but not both of them. Recently, the SST turbulence model with automatic wall function has become the center of attention in the CFD analysis. Menter et al. and Vieser et al. have concluded that SST turbulence model is capable to produce high accuracy results over a wide range of heat transfer cases and the model has been proven for its capability in predicting the flow separation under adverse pressure gradients precisely by adding transport effects into the formulation of eddy-viscosity (Menter et al. 2003, Vieser et al. 2002, Bardina et al. 1997). The SST turbulence model is similar to the k-ε turbulence model for free shear flows and it can overcome deficiencies in the k-ω and BSL k-ω turbulence model. Nonetheless, the SST turbulence model has its advantages in the low Reynolds number computations. The SST turbulence model will give a better prediction for laminar to turbulent flow and also near wall boundary conditions as well as wall shear and heat transfer behavior (Ansys. 2010). The performance of the SST turbulence model has been validated by a large number of case studies (Bardina et al. 1997). The details of the SST turbulence model can be found in the following studies conducted by Menter et al., (2003), Sparrow et al. (2009)

and Lee et al, (2013). Therefore, the SST turbulence model is selected for the current study (Ansys. 2010, Fan et al. 2014, Wu et al. 2010, and Sharma et al. 2015).

Hybrid meshing technique is used to discretize the straight-channel and segmented micro-channel domain into 2,376,444 and 6,495,016 elements using ANSYS ICEM CFD 17.2. Water is used as a cooling fluid and mass flow boundary condition is assigned to the inlet. Physical properties of the water and copper block used in the CFD simulation are tabulated in Table 3.1.

Table 3.1 Physical properties of water and copper used in the simulation

Material	ρ, kgm^{-3}	k, $Wm^{-1}K^{-1}$	C_p, $Jkg^{-1}K^{-1}$	μ, $kgm^{-1}s^{-1}$
Water	997	0.6069	4181.7	0.0008899
Copper	8933	401	385	-

The inlet temperature of the water is kept at 30 ^{o}C. On top of that, the pressure boundary condition is assigned to the outlet. Uniform heat generation of 800 W is applied to the bottom surface of the micro-channel heat sink. Contact resistance present between the heater and micro-channel heat sink is not modeled in this study. The confining walls on the micro-channel test rig are specified as non-slip and adiabatic wall boundary conditions. The computational domain is initialized with 10 kPa pressure condition. Boundary details and setting used for the micro-channel heat sink are tabulated in Table 3.2. Simulation is executed with a high-resolution scheme and first-order turbulence numeric. The convergence criteria for continuity, momentum, and energy (H-energy and T-energy) are set to 1.0×10^{-6}. Workstation with Intel i7-6800K, 3.4 GHz CPU and 64 GB DDR4 RAM is used to perform the

simulation and the total computational time is about 8 hours.

Table 3.2 Boundary details and settings for the micro-channel in CFD analysis

Boundary Name	Boundary details	Value
Inlet	Temperature	30 ºC
	Turbulence Intensity	5%
Outlet	Pressure outlet	0 Pa
Fluid domain	Non-contact wall	Nonslip
	Non-contact wall heat Transfer	Adiabatic
	Turbulence option	SST model
Micro-channel domain	Initial temperature	30 ºC
	Non-contact wall heat transfer	Adiabatic
Heat source domain	Initial temperature	30 ºC
	Non-contact wall heat transfer	Adiabatic
Holder domain	Initial temperature	30 ºC
	Non-contact wall heat Transfer	Adiabatic

3.3.1 Grid Independent test

Grid-independent test is first conducted to ensure that the mesh of the micro-channel heat sink is appropriate to provide a reliable result for heat transfer and flow characterization. The percentage of deviation of the analysis results must be less than 5 % in order to ensure that the results are not affected by further mesh refinement. In the present study, five different mesh configurations, namely mesh-1 (coarse), mesh-2 (medium), mesh-3 (fine), mesh-4 (finer) and mesh-5 (finest) are used to assess the grid quality on the accuracy of the simulation results. The test results are summarized in Table 3.3.

Table 3.3 Grid Independent test result for straight micro-channel and segmented micro-channel

Mesh No	Straight Channel			Segmented		
	Number Of Element	Average temperature, ^{o}C	Pressure drop, Pa	Number of element	Average temperature, ^{o}C	Pressure drop, Pa
Mesh-1	604,126	95.57	2800.56	2,331,419	52.01	14437.20
Mesh-2	1,302,955	97.55	2636.13	4,389,590	53.49	15127.90
% deviation		2.07 %	5.87 %		2.85 %	4.78 %
Mesh-3	2,376,444	97.58	2588.93	6,495,016	53.32	15630.10
% deviation		0.03 %	1.79 %		0.32 %	3.31 %
Mesh-4	4,227,917	97.48	2542.81	12,069,880	53.39	15515.50
% deviation		0.10 %	1.78 %		0.13 %	0.73 %
Mesh-5	8,539,682	97.60	2566.52	28,963,841	53.45	15631.30
% deviation		0.12 %	0.93 %		0.11 %	0.75 %

The grid independent test is conducted using a mass flow rate of 20 gs^{-1}. Mesh-1, mesh-2, mesh-3, mesh-4 and mesh-5 with 604,126, 1,302,955, 2,376,444, 4,227,917 and 8,539,682 elements, respectively are generated to model the straight-channel heat sink. On the other hand, mesh-1, mesh-2, mesh-3, mesh-4 and mesh-5 with 2,331,419, 4,389,590, 6,495,016, 12,069,880 and 28,963,841 elements, respectively are generated to model the segmented micro-channel heat sink. From Table 3, it is clearly shown that the average temperature and pressure drop for the straight-channel are almost constant for five different mesh systems. The variation in average temperature for straight-channel is about 2.07 % from mesh-1 to mesh-2, 0.03 % from mesh-2 to mesh-3, 0.10 % from mesh-3 to mesh-4 and 0.12 % from mesh-4 to mesh-5. Furthermore, the variation in the pressure drop for straight-channel is about 5.87 % from mesh-1 to mesh-2, 1.79 % from mesh-2 to mesh-3, 1.78 % from mesh-3 to mesh-4 and 0.93 % from mesh-4 to mesh-5. Hence, mesh-5 with 8,539,682 elements is sufficient to characterize the performance of the straight channel. A similar trend is also observed for the average temperature and pressure drop development in the segmented micro-channel. The variation in average temperature for segmented micro-channel is about 2.85 % from mesh-

1 to mesh-2, 0.32 % from mesh-2 to mesh-3, 0.13 % from mesh-3 to mesh-4 and 0.11 % from mesh-4 to mesh-5. The variation of pressure drop is about 4.78 % from mesh-1 to mesh-2, 3.31 % from mesh-2 to mesh-3, 0.73 % from mesh-3 and mesh-4 and 0.75 % from mesh-4 to mesh-5. Therefore, segmented micro-channel with 28,963,841 elements is sufficient to characterize the heat transfer and flow performance.

3.4 Optimization

3.4.1 Taguchi method

The Taguchi method was first introduced by Genichi Taguchi to improve the process and product quality based on statistical concepts and tools. This method helps to identify the possible combinations of a factor to produce the best solution at minimum cost and time (Taguchi. 1987 and Kotcioglu et al. 2013). In the current study, the Taguchi method is applied to determine the micro-channel design parameters that will improve the thermal performance and flow characteristics to derive an optimized micro-channel design. Instead of using full factorial analysis which requires a total of 729 runs of the simulation, the orthogonal array L_{27}, which consists of six three-level factors and a total of 27 runs is used to optimize the segmented micro-channel heat sink. Genetic algorithm is one of the optimization method that can be used to optimized micro-channel heat sink. Genetic algorithm use the combination of the best known hypothesis and natural selection to optimized. Yan et al. study the Y-shaped fractal network using four branching level

known to offers better thermal performance with lower manufacturing difficulty (Yan et al. 2019). In this research, due to inadequate research material, the parameter selection was set theoretically within range and optimized further to understand the design of micro-channel heat sink. Therefore, Taguchi method optimization was more suitable for this research. The noise factor is not considered in the analysis. The factor level used to optimize the segmented micro-channel is tabulated in Table 3.4. In total there are six different factors considered in this study, such as fin width (W), fin length (L), fin transverse length (T), number of segments, channel width (C) and mass flow rate. The aim of this optimization process is to obtain maximum specific performance, minimum pressure drop and minimum variation of temperature and the orthogonal array simulation plan is tabulated in Table 3.5.

Table 3.4 Taguchi method optimization parameter study

Factor		Level		
		1	2	3
A	Fin width (W), mm	4	2	1
B	Fin length (L), mm	4	2	1
C	Fin transverse distance (T), mm	5	3	2
D	Number of segments	3	2	1
E	Channel width (C), mm	1	0.5	0.3
F	Mass flow rate, gs^{-1}	20	15	10

Table 3.5 Taguchi method simulation plan-L_{27}

Run	Parameter and its levels					
	A	B	C	D	E	F
1	1	1	1	1	1	1
2	1	1	1	1	2	2
3	1	1	1	1	3	3
4	1	2	2	2	1	1
5	1	2	2	2	2	2
6	1	2	2	2	3	3
7	1	3	3	3	1	1
8	1	3	3	3	2	2
9	1	3	3	3	3	3
10	2	1	2	3	1	2
11	2	1	2	3	2	3
12	2	1	2	3	3	1
13	2	2	3	1	1	2
14	2	2	3	1	2	3
15	2	2	3	1	3	1
16	2	3	1	2	1	2
17	2	3	1	2	2	3
18	2	3	1	2	3	1
19	3	1	3	2	1	3
20	3	1	3	2	2	1
21	3	1	3	2	3	2
22	3	2	1	3	1	3
23	3	2	1	3	2	1
24	3	2	1	3	3	2
25	3	3	2	1	1	3
26	3	3	2	1	2	1
27	3	3	2	1	3	2

3.4.2 Signal to noise ratio

A loss function is used in the Taguchi method to calculate the deviation between simulation results and the desired value. This loss function is then converted to Signal-to-Noise ratio (SNR). There are three different types of quality characteristic concerning the target design in the Taguchi method analysis, which are known as “Larger the best”, “Nominal the best” and “Smaller the best” as described in Eq. 3-6- Eq. 3-8 (Sahin et al. 2005 and

Kotcioglu et al. 2013). Since the aim of the study is to achieve higher heat transfer performance with minimum pressure drop and variation of temperature, it is desired to have the highest value for the specific performance and lowest value for the pressure drop and variation of temperature. Therefore, "Larger the best" as in Eq. 3-6 will be used for specific performance and "smaller the best" will be used for the pressure drop and variation of temperature. A high value of η indicates a good performance (Sahin et al. 2005 and Taguchi. 1987).

Larger the best

$$\eta = -10 \log_{10} \left(\frac{1}{n} \sum_{i=1}^{n} \frac{1}{Y_i^2} \right) \tag{3-6}$$

Smaller the best

$$\eta = -10 \log_{10} \left(\frac{1}{n} \sum_{i=1}^{n} Y_i^2 \right) \tag{3-7}$$

Nominal the best

$$\eta = -10 \log_{10} \left(\frac{1}{n} \sum_{i=1}^{n} \frac{\mu^2}{\sigma^2} \right) \tag{3-8}$$

Y_i Performance value of the simulation i^{th}.

n Number of simulation run.

3.4.3 Analysis of variance (ANOVA)

The Analysis of variance (ANOVA) is used to analyze the results of the orthogonal array experiment to identify the effect contributed by each factor (Roy. 2001 and Ross. 1996). It is also an important technique to analyze the effect of unconditional factors on a response. In this study, the design parameters that can reduce the variation are identified by assessing the amount of variation in the responses through ANOVA. In the Taguchi method, there are three different types of target design that consider as signal to noise ratio. The quality of the product will be improved if the signal to noise ratio is high. In this study, "Larger the best" is used as the optimization criteria for specific performance while "smaller the best" is used as the optimization criteria for pressure drop and variation of temperature. Lastly, the contribution ratio for each design parameters is determined through ANOVA analysis. The influence of each factor on the performance of the micro-channel heat sink can be identified from the percentage of contribution of each control factor. Fisher test (F-test) with 95 % of confidence level ($P < 0.05$) is used to assess the significance of individual parameter on specific performance, pressure drop and variation of temperature. Variance of the corresponding parameter is compared with residual variance and estimated as the mean square of the parameter to the mean square of variance to derive the F-value for F-test. F-value is usually taken when it is greater or equal to unity. When P-value is less than 0.05, the parameter is considered to have a significant effect on the performance characteristics and vice versa (Adewale et al. 2017).

3.4.4 Grey Relational Analysis (GRA)

Grey Relational Analysis (GRA) applies the information from the grey system to evaluate the design parameters qualitatively for multiple performance characteristics. Level of similarity and variability in the design parameters are the fundamental components of GRA (Tsai et al. 2003). For example, it is desired to have the highest specific performance and lowest pressure drop and variation of temperature simultaneously for this study. The optimization of the segmented micro-channel heat sink is performed in the following steps:

1. The simulation results of the specific performance are normalized according to Eq. 3-9 while pressure drop and variation of temperature are normalized according to Eq. 3-10.
2. The grey relational coefficient (GRC) is calculated according to Eq. 3-11.
3. The grey relational grade (GRG) is calculated according to the weighting assigned for specific performance, pressure drop and variation of temperature as in Eq. 3-12. The highest GRG among all candidate schemes will be the best choice, while the priority of all other candidates can be easily sequenced by their GRG value.

There are three different criteria for normalization such as largest the best, nominal the best and smaller the best. However, only two criteria are used which is larger the best for specific performance and smaller the best for

pressure drop and variation temperature. The simulation results are normalized to a range between 0 and 1 according to Eq. 3-9 and Eq. 3-10 (Wu. 1996).

Larger the best:

$$x_i^*(k) = \frac{x_i^0(k) - \min x_i^0(k)}{\max x_i^0(k) - \min x_i^0(k)} \quad (3\text{-}9)$$

Smaller the best:

$$x_i^*(k) = \frac{\max x_i^0(k) - x_i^0(k)}{\max x_i^0(k) - \min x_i^0(k)} \quad (3\text{-}10)$$

$x_i^0(k)$ is the normalized value of the k^{th} element in the i^{th} sequence.

$\max x_i^0(k)$ is the largest value of $x_i^0(k)$.

$\min x_i^0(k)$ is the smallest value of $x_i^0(k)$.

Next, the Grey Relational Coefficient (GRC) is computed. The grey coefficient is defined by the equation below:

$$\xi_i(k) = \frac{\Delta_{min} + \psi\Delta_{max}}{\Delta_{0i}(k) + \psi\Delta_{max}} \quad (3\text{-}11)$$

Δ_{0i} is the deviation sequence between the reference sequence and the comparable sequence with $x_0^*(k) = 1$.

$$\Delta_{0i} = \|x_0^*(k) - x_i^*(k)\|,$$

$$\Delta_{min} = \min_{\forall j \in i} \min_{\forall k} \|x_0(k) - x_j(k)\|,$$

$$\Delta_{max} = \max_{\forall j \in i} \max_{\forall k} \|x_0(k) - x_j(k)\|,$$

$x_0^*(k)$ is the referential sequence;

$x_i^*(k)$ is the comparative sequence;

Δ_{min} Smallest value of Δ_{0i}, 0.

Δ_{max} Largest value of Δ_{0i}, 1.

ψ is the distinguishing or identification coefficient with $0 \leq \Psi \leq 1$, the value depends on the requirements of the real system. The value is chosen to magnify the difference between the relational coefficients. In general, $\psi = 0.5$ is used (Dey et al. 2017).

Finally, Grey Relational Grade (GRG) as in Eq. 12 is calculated after deriving the GRC value. The GRG is taken as a single representative of the multiple quality responses (Dey et al. 2017).

$$\gamma_i = \frac{1}{\sum_{k=1}^{n} w_k} \sum_{k=1}^{n} w_k \xi_i(k) \tag{3-12}$$

where

γ_i Overall grey relational grade for i^{th} experiment.

w_k Normalized weight value of k^{th} performance characteristic.

Table 3.6 Normalized weight value each response

Weightage	Response		
	Specific performance (SP)	Pressure drop (PD)	Temperature variation (TV)
w	0.3	0.3	0.4

3.4.5 Data Processing

The heat transfer from the micro-channel heat sink to the water can be calculated using Eq. 3-13 and Eq. 3-14 (Sahin et al. 2005 and Saw et al. 2016):

$$\dot{Q}_{total} = \dot{Q}_{conv} + \dot{Q}_{rad} + \dot{Q}_{loss} \quad (3\text{-}13)$$

where

$$\dot{Q}_{conv} = \dot{m} C_p (T_{out} - T_{in}) \quad (3\text{-}14)$$

$\dot{Q}_{conv}$ Amount of heat dissipated through convection, W

$\dot{Q}_{rad}$ Amount of heat dissipated through radiation, W

$\dot{Q}_{loss}$ Amount of heat loss due to poor insulation, W

$\dot{m}$ Mass flow rate of water, $kg.s^{-1}$

C_p Specific heat capacity of water, $J.kg^{-1}.K^{-1}$

T_{out} Outlet temperature, K

T_{in} Inlet temperature, K

The heat transfer from the micro-channel heat sink by convection can be calculated by Eq. 3-15 (Sahin et al. 2005 and Saw et al. 2016):

$$\dot{Q}_{conv} = \bar{h} A_s \left[\bar{T}_s - \left(\frac{T_{out} + T_{in}}{2} \right) \right] \quad (3\text{-}15)$$

$\bar{h}$ Convection heat transfer coefficient, $W.m^{-2}.K^{-1}$

A_s Total heat transfer area, m^2

$\bar{T}_s$ Average surface temperature, K

In this study, radiative heat loss is neglected, and it is also assumed that the test section is well insulated. Hence, second and last terms in Eq. 3-16 are neglected and Eq. 16 can be further reduced to

$$\dot{Q}_{total} = \dot{Q}_{conv} \tag{3-16}$$

As a result, the heat transfer rate to the water is equal to the heat loss from the micro-channel heat sink.

$$\bar{h} = \frac{\dot{Q}_{conv}}{A_s \left[\bar{T}_s - \left(\frac{T_{out} + T_{in}}{2}\right)\right]} \tag{3-17}$$

The Nusselt number is calculated using the Eq. 3-18:

$$Nu = \frac{\bar{h} D_h}{k} \tag{3-18}$$

D_h Hydraulic diameter, m

k Thermal conductivity of water, $W.m^{-1}.K^{-1}$

Hydraulic diameter is calculated using the equation below:

$$D_h = \frac{4V_f}{A_f} \tag{3-19}$$

V_f Total fluid volume inside the heat sink, m^3

A_f Total convective heat transfer area in contact with the fluid, m^2

The Reynolds number for the cooling fluid is computed using Eq. 3-20 (Sahin et al. 2005 and Kays et al. 1964):

$$Re = \frac{\rho U_\infty D_h}{\mu} \tag{3-20}$$

ρ Density of water, kg.m^{-3}

U_∞ Inlet velocity of water, m.s^{-1}

μ Dynamic viscosity of water, kg.m^{-1}.s^{-1}

The friction factor (f) of the micro-channel is defined by Eq. 3-21 (Kays et al. 1964):

$$f = \frac{A_c}{A_s} \frac{2\Delta p\, \rho}{G^2} \tag{3-21}$$

Δp Pressure drop through heat sink, Pa

ρ Density of water, kg.m^{-3}

A_c Free flow area, m^2

G Mass flux of water based on minimum flow area, $\left(\frac{\dot{m}}{A_c}\right)$ kg.m^{-2}s^{-1}

A_c/A_s Ratio of free flow area to total heat transfer area can be defined as r_h/L

r_h Hydraulic radius, m

L Length of the heat sink, m

For comparison of the different type of heat sink design, specific performance as in Eq. 3-22 is used (Smith. 2005). The formula considers the change of the average temperature of the heat sink per unit volume of heat generated.

$$\dot{Q}_{spec} = \frac{\dot{Q}}{V\Delta\theta} \tag{3-22}$$

$\dot{Q}$ Amount of heat generated, W

V Volume of the heat sink, m^3

$\Delta\theta$ Change of temperature, K

The thermal resistance of the heat sink can be calculated using the equation below (Lie et al. 2007):

$$\theta = \frac{T_{max} - T_{in}}{Q} \tag{3-23}$$

T_{max} Maximum bottom temperature, K

T_{in} Inlet fluid temperature, K

Q Total heat generation, W

Pumping power consumed to deliver the flow needed is defined using Eq. 3-24 (Lie et al. 2007).

$$W_{pp} = \dot{V}\,\Delta p \tag{3-24}$$

$\dot{V}$ Volumetric flow rate, m^3s^{-1}

3.5 Experimental Setup

Numerical simulation required validation with the experimental data. Thus, the test rig is developed to characterize the thermal performance of the novel heat sink design. Segmented micro- channel heat sink design is based on the result obtained from the optimization and experimental setup as shown in Fig 3.2.

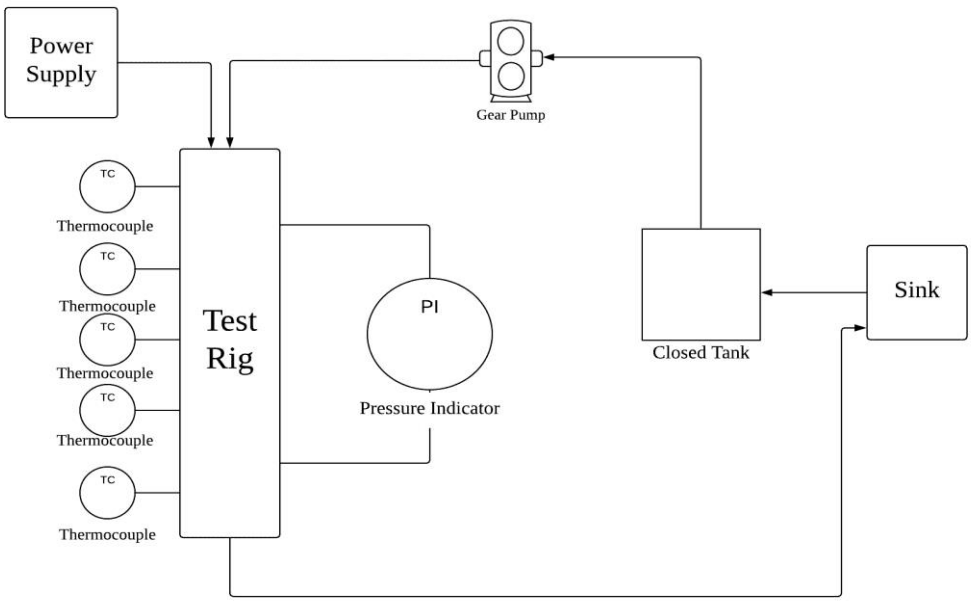

Fig 3.2 Experimental setup for experimental analysis

3.5.1 Test rig design

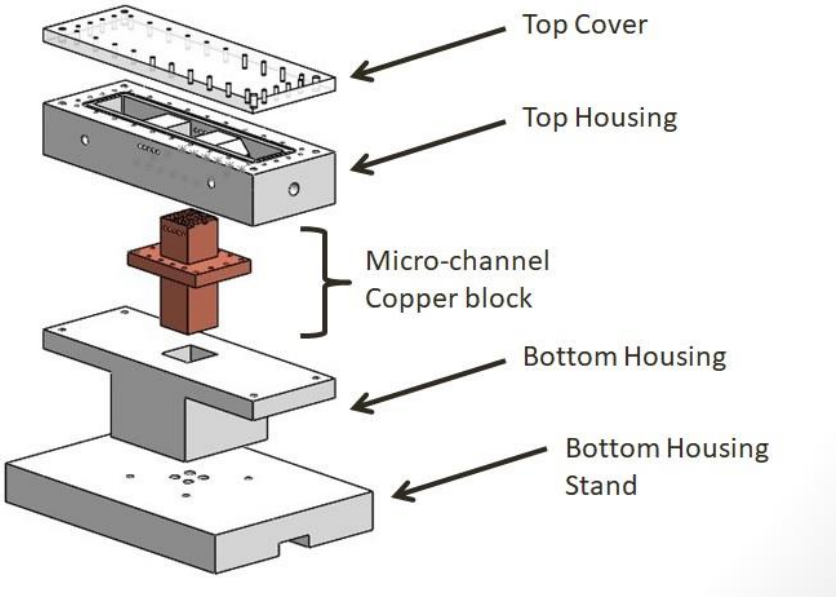

Fig 3.3 Test rig design

Test rig used for the experimental work consists of 5 different parts which can be divided into top cover, top housing, micro-channel copper block, bottom housing, and bottom housing stand as shown in Fig 3.3. The top cover is made of perspex, while top housing, bottom housing, and bottom housing stand are made of Teflon. In the test rig, the copper block is used to fabricate micro-channel heat sink as shown in Fig 3.4. At the bottom of the copper block, four holes with a diameter of 3.9 mm are prepared to insert cartridge heaters to heat up the micro-channel.

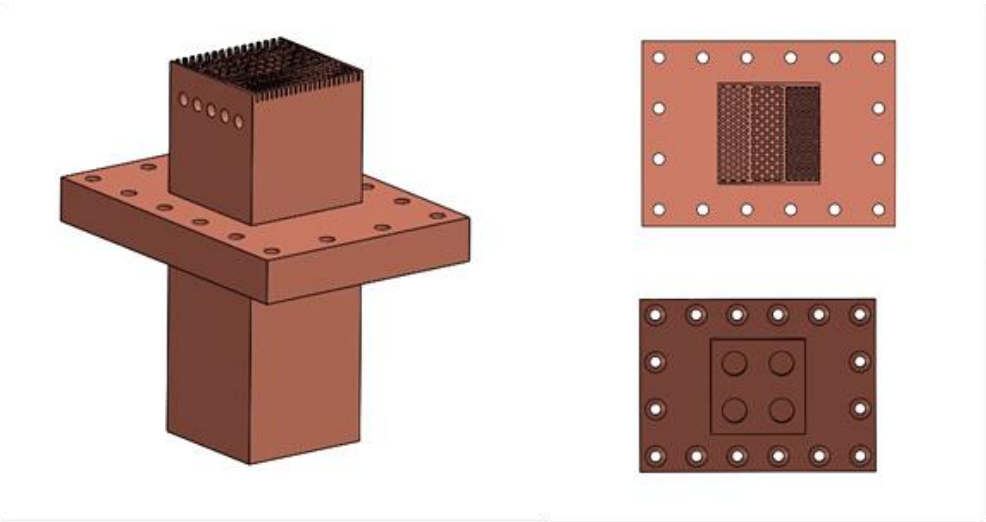

Fig 3.4 Micro-channel heat sink

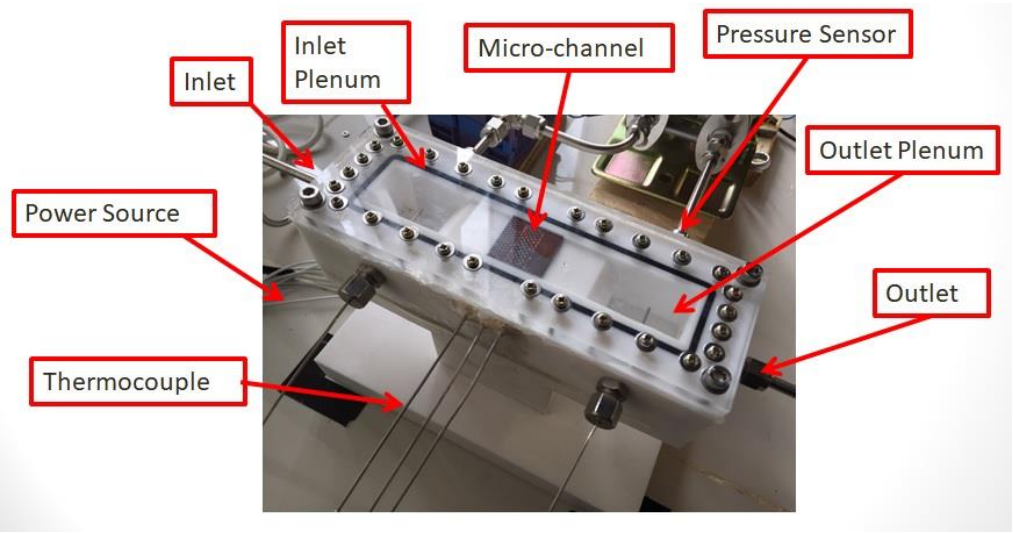

Fig 3.5 Micro-channel test rig

Fig 3.5 shows the test rig of the micro-channel heat sink experiment. Inlet and outlet plenum is used to create a stable flow to the micro-channel heat sink. Pressure transmitter (ABB 266MST) as shown in Fig 3.6 is installed at the inlet and outlet plenum to measure the pressure drop across the micro-channel. Besides, five K-type thermocouples are installed 3mm below the micro-channel to measure the temperature across the micro-channel and

connected to the data logger. 4 cartridge heaters are installed beneath of the micro-channel to provide a heat source for micro-channel. Gear pump (ISMATEC MCP-Z) as shown in Fig 3.7 is used to supply cooling fluid to the micro-channel test rig.

Fig 3.6 Pressure transmitter

Fig 3.7 Gear Pump

3.6 Summary

This chapter explains the methodology of the current study which encompassed numerical modeling, optimization and experimental setup. Besides the design and optimization parameters are also discussed in details. Furthermore, the type of equipment and sensors used to measure the experimental results are also reviewed.

CHAPTER 4

RESULTS

4.1 Introduction

In this chapter, results obtained from the simulation and experimental is tabulated and analyzed to understand the thermal performance and flow field of the novel micro-channel heat sink and conventional straight channel heat sink.

4.2 Straight Channel

Evolution of the average surface temperature and variation of temperature on the heated surface for the straight-channel is illustrated in Fig. 4.1. It is ascertained that the average surface temperature and variation of temperature are inversely proportional to the mass flow rate of water. In order to achieve an operating temperature which is less than 85 ^{o}C, at least 40 gs^{-1} of water is required. However, the recorded temperature variation is very high, which is about 13.2 ^{o}C. This may be attributed to the continuous development of the thermal boundary layer in the straight channel. Hence, a higher flow rate is necessary in order to subdue the development of thermal boundary layer effect. As shown in Fig. 4.1, at least 100 gs^{-1} of water is needed to achieve a temperature difference of about 4.5 ^{o}C.

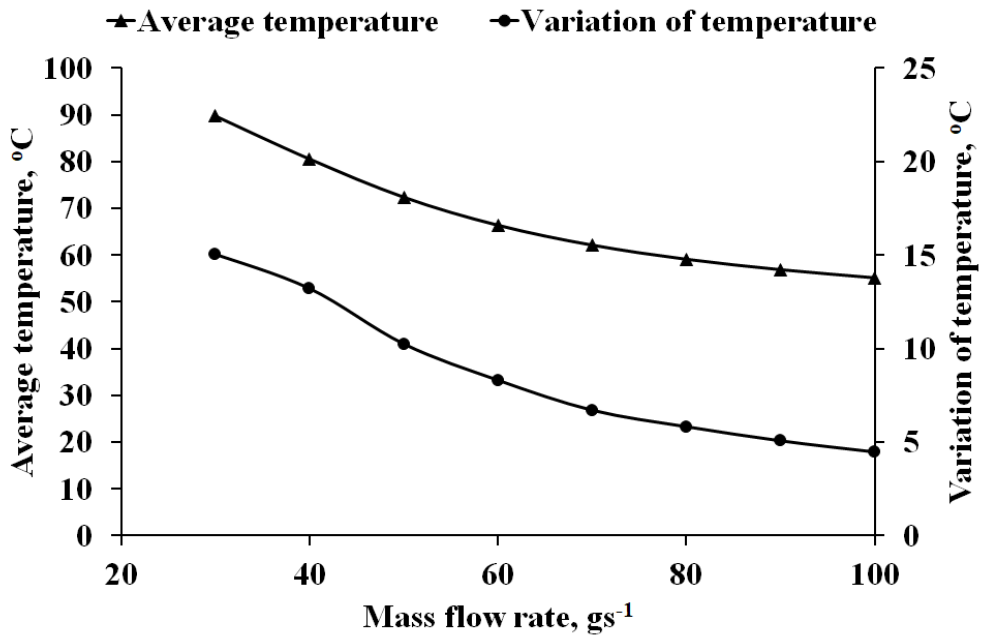

Fig 4.1 Evolution of the average surface temperature and variation of temperature on the heated surface for the straight-channel

Temperature contour plot of the straight-channel at 100 gs^{-1} of water is illustrated in Fig. 4.2. The maximum and minimum temperatures of the straight-channel heat sink are recorded at 56.8 ^{o}C and 52.3 ^{o}C, respectively. The variation of temperature across the micro-channel is approximately 4.5 ^{o}C.

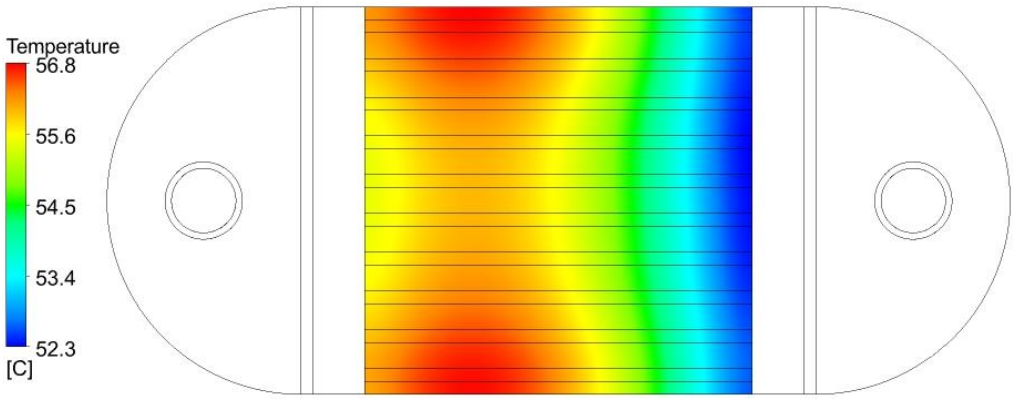

Fig 4.2 Temperature contour plot of the straight-channel at 100 gs^{-1} of water

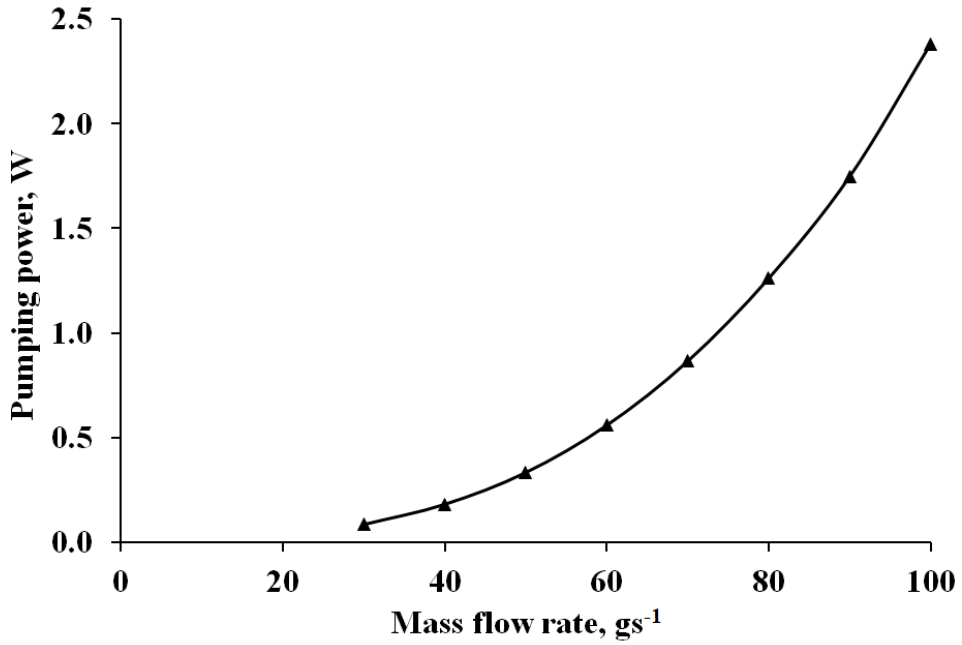

Fig 4.3 Pumping power for straight-channel

Besides, higher pumping power is needed to push the coolant through the straight-channel. In calculating the pumping power, Eq. 3-24 was used. This is further evidenced by the pumping power versus mass flow rate of water plot in Fig. 4.3. It is shown that the pumping power needed for the straight-channel is exponentially increasing with the mass flow rate of the coolant. At a flow rate of 100 gs^{-1}, the required pumping power is about 2.38 W.

4.3 Segmented micro-channel

It is always a challenging task to simultaneously increase the heat transfer rate while at the meantime, reduce the pressure drop and temperature variation in a micro-channel heat sink. Therefore, specific performance, pressure drop and temperature variation of the segmented micro-channel need to be explored.

The considered design parameters are fin width, fin length, fin transverse length, number of segments, channel width, and different mass flow rate. Each design parameter has three levels as stated in Table 3.4. Hence, a systematic approach is used to analyze the simulation results by constructing a simulation plan for the segmented micro-channel. In order to produce an optimized design, the simulation results are analyzed to determine the effect each design parameter on the specific performance, pressure drop and temperature variation. The simulation results are further converted to signal to noise ratio for the analysis purpose. The signal to noise ratio for the specific performance, pressure drop and variation of temperature is tabulated in Table 4.1

Table 4.1 Simulation plan of L_{27} (3^6) for specific performance, pressure drop and temperature variation with their SNR values

Run	A	B	C	D	E	F	Specific performance	SNR	Pressure drop	S-N	Temperature variation	SNR
1	1	1	1	1	1	1	6783421	136.63	16515	-84.36	5.5	-14.82
2	1	1	1	1	2	2	8006979	138.07	14060	-82.96	5.2	-14.24
3	1	1	1	1	3	3	5632229	135.01	10102	-80.09	6.6	-16.38
4	1	2	2	2	1	1	6486681	136.24	17259	-84.74	6.2	-15.87
5	1	2	2	2	2	2	7851987	137.90	18312	-85.25	13.0	-22.26
6	1	2	2	2	3	3	5621733	135.00	18239	-85.22	17.4	-24.83
7	1	3	3	3	1	1	6403662	136.13	21260	-86.55	14.2	-23.07
8	1	3	3	3	2	2	7247409	137.20	34164	-90.67	12.1	-21.64
9	1	3	3	3	3	3	6527874	136.30	41540	-92.37	14.0	-22.92
10	2	1	2	3	1	2	6114567	135.73	7316	-77.29	12.1	-21.62
11	2	1	2	3	2	3	6272901	135.95	7716	-77.75	14.3	-23.09
12	2	1	2	3	3	1	8903969	138.99	64043	-96.13	7.2	-17.18
13	2	2	3	1	1	2	8789857	138.88	10560	-80.47	4.3	-12.71
14	2	2	3	1	2	3	7360159	137.34	5614	-74.99	9.8	-19.80
15	2	2	3	1	3	1	8336032	138.42	29666	-89.45	5.7	-15.16
16	2	3	1	2	1	2	8405935	138.49	12636	-82.03	9.3	-19.37
17	2	3	1	2	2	3	6055831	135.64	7974	-78.03	15.3	-23.68
18	2	3	1	2	3	1	8181100	138.26	49828	-93.95	11.2	-20.97
19	3	1	3	2	1	3	5029866	134.03	2412	-67.65	9.4	-19.48
20	3	1	3	2	2	1	7358597	137.34	10183	-80.16	12.3	-21.79
21	3	1	3	2	3	2	6877786	136.75	7179	-77.12	17.0	-24.61
22	3	2	1	3	1	3	4857748	133.73	789	-57.95	11.8	-21.42
23	3	2	1	3	2	1	7924423	137.98	5365	-74.59	6.8	-16.60
24	3	2	1	3	3	2	7995436	138.06	6517	-76.28	8.5	-18.60
25	3	3	2	1	1	3	5904962	135.42	3741	-71.46	4.7	-13.35
26	3	3	2	1	2	1	8176043	138.25	16222	-84.20	5.7	-15.06
27	3	3	2	1	3	2	7664773	137.69	11138	-80.94	10.0	-20.04

The response diagram for the design parameter on the specific performance, pressure drop, and temperature variation are shown in Fig. 4.4, Fig. 4.5 and Fig. 4.6, respectively. On the other hand, the contribution ratio of each design parameter on the specific performance, pressure drop, and temperature variation are illustrated in Fig. 4.7. The larger slope in the figure indicates that the design parameter has a more significant impact on the performance characteristic. Based on the results shown in Fig. 4.4 and Fig. 4.7, the most influential parameters on the specific performance are ranked as follows: mass flow rate (F) at level 2 (15 gs^{-1}), channel width (E) at level 3 (0.3 mm), fin width (A) at level 2 (2 mm), number of segments (D) at level 1 (3), fin length (B) at level 3 (1 mm) and fin transverse distance (C) at level 3 (2 mm). The specific performance is enhanced by increasing the mass flow rate of water, as well as reducing the channel width and fin width. The maximum specific performance is obtained at 15 gs^{-1} of water, 0.3 mm of channel width and 2 mm of fin width. Besides, it is also observed that the specific performance does not change significantly with the transverse distance between the fins and follow by the number of segments present in the segmented micro-channel heat sink. Therefore, the optimal parameter setting for the maximum specific performance is A2B3C3D1E3F2.

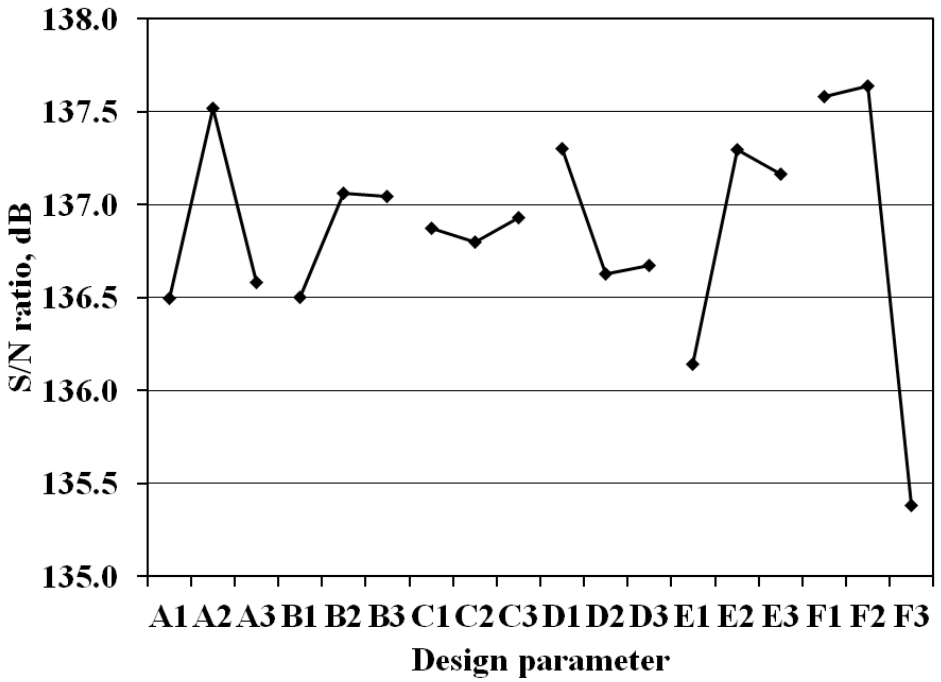

Fig 4.4 Response diagram for the design parameter on the specific performance

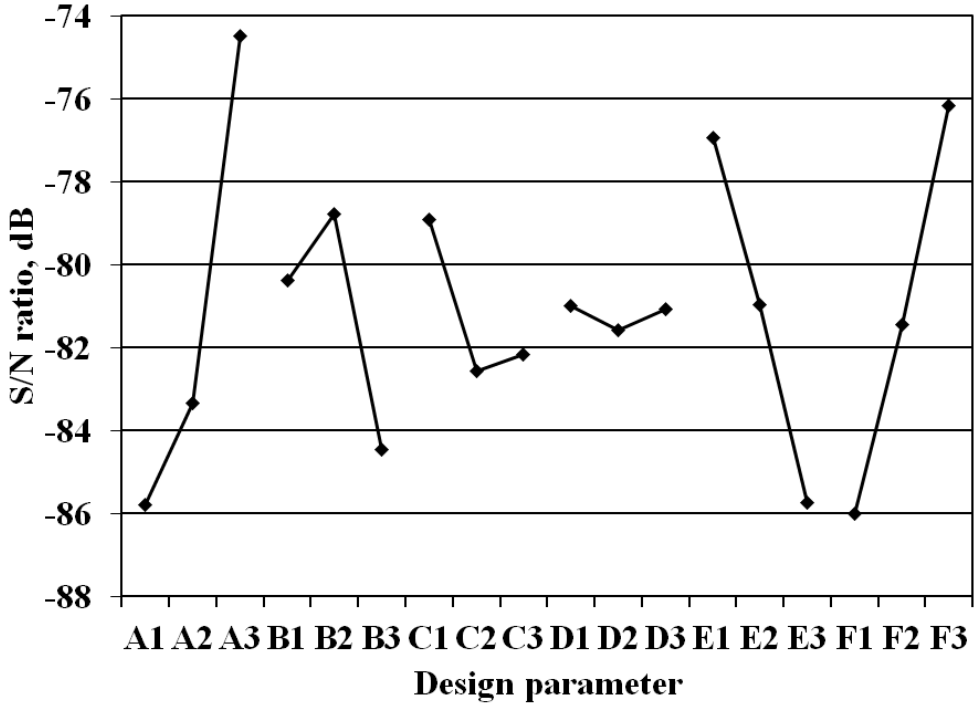

Fig 4.5 Response diagram for the design parameter on the pressure drop

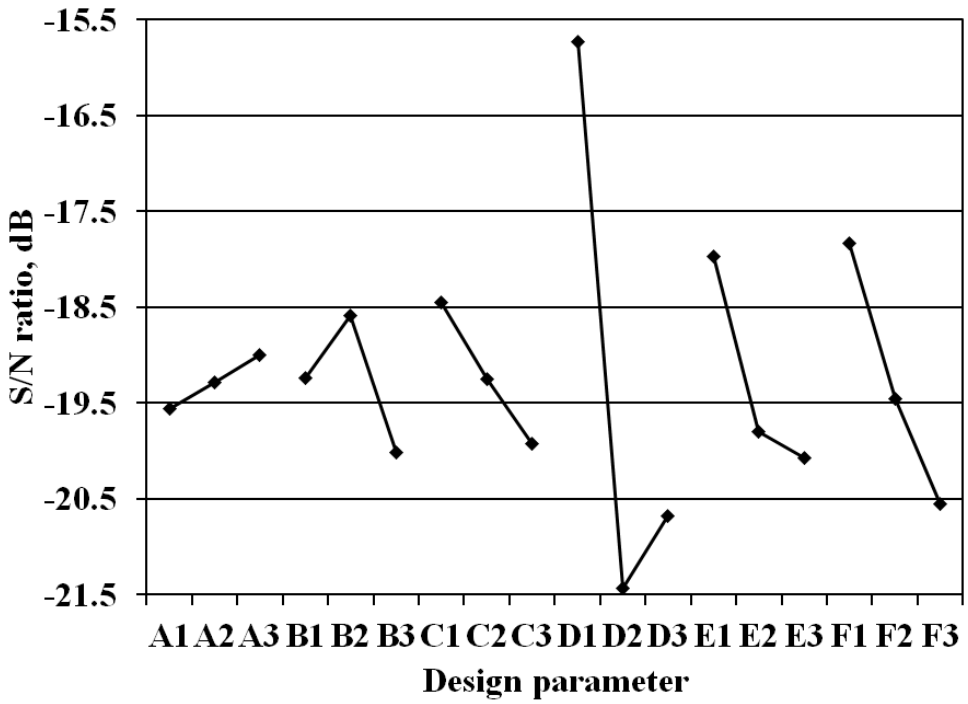

Fig 4.6 Response diagram for the design parameter on the temperature variation

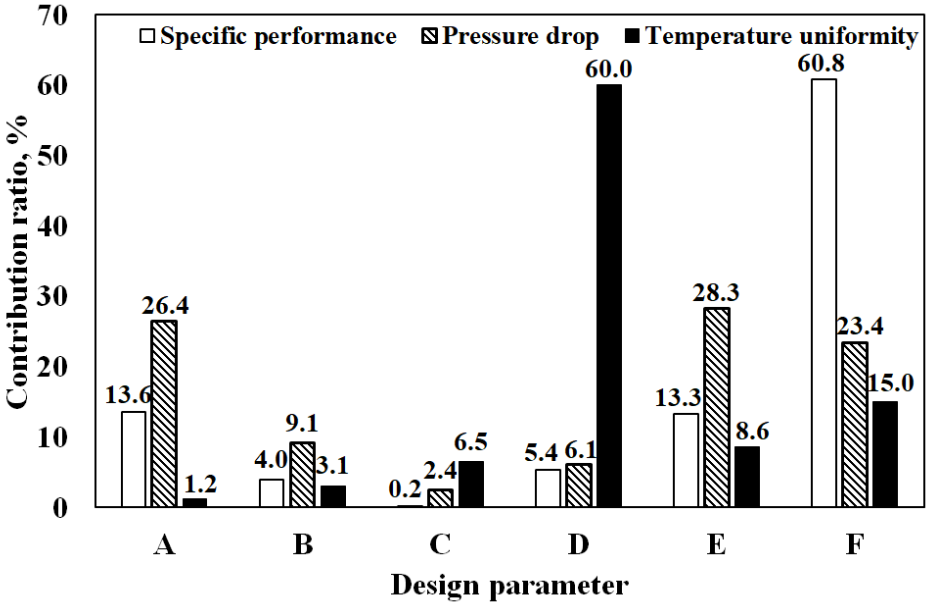

Fig 4.7 Contribution ratio of each design parameter on the specific performance, pressure drop and temperature variation

According to the results depicted in Fig. 4.5 and Fig. 4.7, the most effective design parameters with respect to the pressure drop are as follows: fin width (A) at level 3 (1 mm), mass flow rate (F) at level 3 (10 gs^{-1}), channel width (E) at level 1 (1 mm), fin length (B) at level 2 (2 mm), fin transverse distance (C) at level 1 (5 mm) and number of segments (D) at level 1 (3). The pressure drop dramatically decreases as a result of reducing the fin width, reducing the flow rate of water and increasing channel width. Minimum pressure drop is obtained when the fin width is 1 mm, the mass flow rate is 10 gs^{-1} and the channel width is 1 mm. Furthermore, it is also noticed that a number of segments do not affect the pressure drop significantly. Although there is no important change in the pressure drop, a micro-channel heat sink with three segments is the optimum setting for the pressure drop parameter. Hence, the optimal parameter setting for the minimum pressure drop is A3B2C1D1E1F3.

According to Fig. 4.6 and Fig. 4.7, the most influential parameters on the temperature variation are arranged as follows: number of segments (D) at level 1 (3), mass flow rate (F) at level 1 (20 gs^{-1}), channel width (E) at level 1 (1 mm), fin transverse distance (C) at level 1 (5 mm), fin length (B) at level 2 (2 mm) and fin width (A) at level 3 (1 mm). The variation of temperature reduces with a higher number of segments, the higher mass flow rate of water and longer channel width. The minimum variation of temperature is achieved when the number of the segment is three, the mass flow rate is 20 gs^{-1} and the channel width is 1 mm. Furthermore, it is also observed that the width of the fin does not affect the variation of temperature significantly. Although the

width of the fin is not an important factor affecting the temperature variation, fin width of about 1 mm is the optimum setting for the minimum variation of temperature. Thus, the optimal parameter setting for the minimum temperature variation is A3B2C1D1E1F1.

Based on the above analysis, it is clearly shown that it is easy to evaluate the effects of optimum design parameters on each of the target response separately. If there are multiple responses involved in the optimization process, there are no single design parameters that can satisfy all the required responses. Hence, a more systematic approach is employed, namely, grey relational analysis, to derive the optimum design parameter to compromise each response by using the weighting method. In this study, a variation of temperature is the most desired response followed by the specific performance and pressure drop. Therefore, the weighting values for specific performance, pressure drop and variation of temperature are set to 0.3, 0.3 and 0.4, respectively.

Firstly, the simulation results are normalized to a range of 0 and 1. Next, the grey relational coefficient and grey relational grade are computed as tabulated in Table 4.2. Finally, the response graph of the grey relational grade according to the L_{27} orthogonal array simulation design plan is plotted in Fig. 4.8. As shown in Fig. 4.10, the most ideal candidate for the optimal design parameters are fin width (A) at level 3 (1 mm), fin length (B) at level 2 (2 mm), fin transverse distance (C) at level 1 (5 mm), number of segments (D) at level 1 (3), channel width (E) at level 1 (1 mm) and mass flow rate (F) at level

2 (15 gs^{-1}). The optimized design parameter for segmented micro-channel heat sink is A3B2C1D1E1F2. In the previous chapter, by mapping the orthogonal array simulation design plan in Table 3.4 with the plots in Fig. 4.8, it is found that the simulations corresponding to the optimum conditions are not performed yet. Hence, a confirmation test is required to be conducted at the optimum design parameters to validate the prediction.

Table 4.2 Normalized response, grey relational coefficients and grey relational grade for the segmented micro-channel.

	Normalized response			GRC			GRG	Orders
Runs	SP	PD	TV	SP	PD	TV		
1	0.476	0.751	0.910	0.488	0.668	0.847	0.686	9
2	0.778	0.790	0.937	0.693	0.704	0.888	0.774	3
3	0.191	0.853	0.827	0.382	0.773	0.743	0.644	13
4	0.403	0.740	0.855	0.456	0.658	0.776	0.644	12
5	0.740	0.723	0.340	0.658	0.643	0.431	0.563	18
6	0.189	0.724	0.000	0.381	0.644	0.333	0.441	26
7	0.382	0.676	0.244	0.447	0.607	0.398	0.476	25
8	0.591	0.472	0.408	0.550	0.487	0.458	0.494	24
9	0.413	0.356	0.263	0.460	0.437	0.404	0.431	27
10	0.311	0.897	0.410	0.420	0.829	0.459	0.558	19
11	0.350	0.890	0.242	0.435	0.820	0.397	0.535	21
12	1.000	0.000	0.778	1.000	0.333	0.693	0.677	10
13	0.972	0.846	1.000	0.947	0.764	1.000	0.913	1
14	0.618	0.924	0.585	0.567	0.868	0.546	0.649	11
15	0.860	0.543	0.893	0.781	0.523	0.823	0.720	6
16	0.877	0.813	0.621	0.802	0.727	0.569	0.686	8
17	0.296	0.886	0.165	0.415	0.815	0.374	0.519	23
18	0.821	0.225	0.477	0.737	0.392	0.489	0.534	22
19	0.043	0.974	0.611	0.343	0.951	0.563	0.613	15
20	0.618	0.851	0.393	0.567	0.771	0.452	0.582	17
21	0.499	0.899	0.034	0.500	0.832	0.341	0.536	20
22	0.000	1.000	0.432	0.333	1.000	0.468	0.587	16
23	0.758	0.928	0.814	0.674	0.874	0.729	0.756	4
24	0.775	0.909	0.681	0.690	0.847	0.610	0.705	7
25	0.259	0.953	0.975	0.403	0.915	0.952	0.776	2
26	0.820	0.756	0.897	0.735	0.672	0.830	0.754	5
27	0.694	0.836	0.564	0.620	0.753	0.534	0.626	14

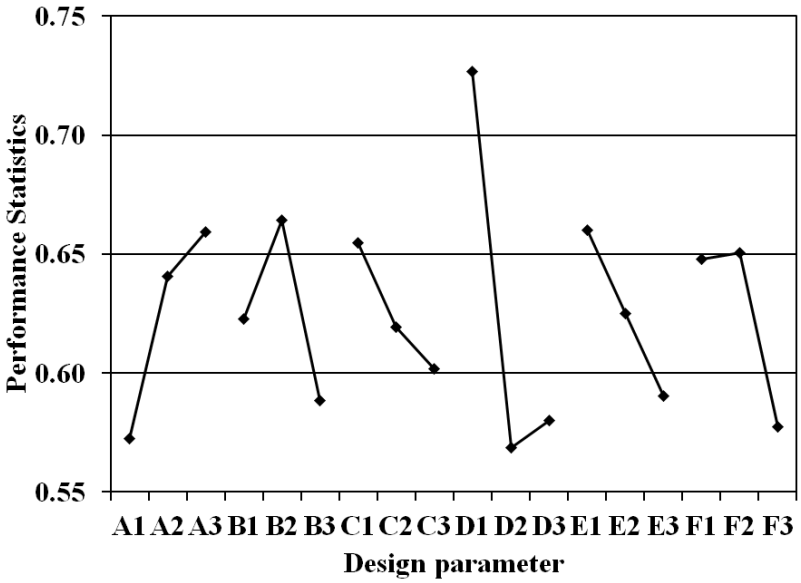

Fig 4.8 Response diagram for the design parameter on the overall performance

Development of the average surface temperature and variation of the temperature of the optimized segmented micro-channel heat sink is illustrated in Fig. 4.9. As expected, the average temperature and the variation of temperature decrease progressively with the mass flow rate of water. 5 gs^{-1} of water is sufficient to reduce the temperature of the heated surface to less than 85 ^{o}C. However, the variation of temperature is still above the desired range which is about 14.6 ^{o}C. In order to achieve the temperature variation that is less than 3 ^{o}C, about 15 gs^{-1} of water is needed and the average temperature of the heated surface will be reduced to approximately 56.6 ^{o}C.

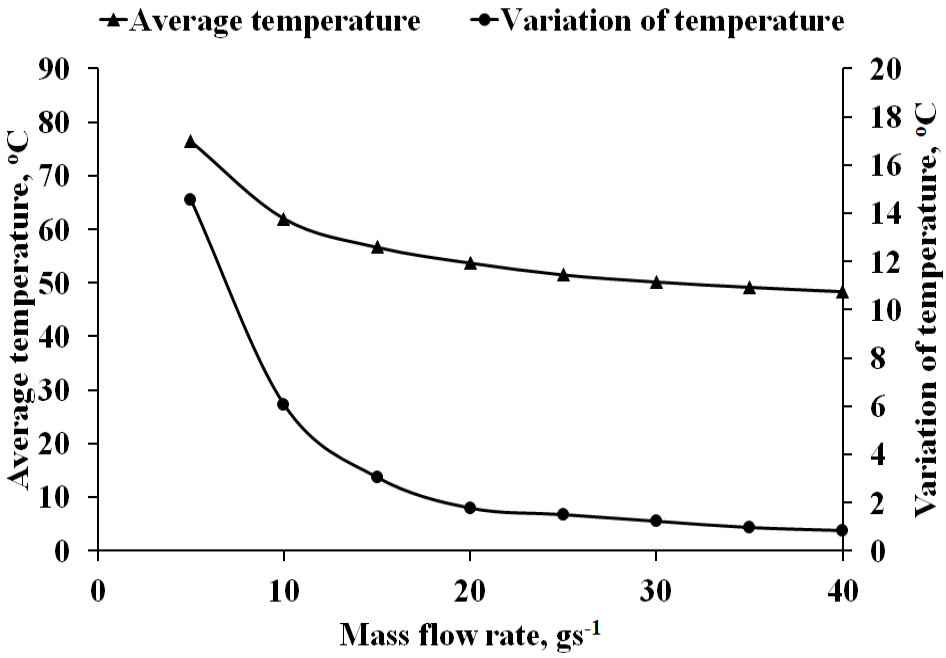

Fig 4.9 Optimized segmented micro-channel heat sink the average surface temperature and variation of temperature

The total heat transfer area in the downstream is inevitably increased and temperature distribution is more uniform and the occurrence of the hot spot will be reduced. Temperature contour plot of the segmented micro-channel heat sink under 15 gs^{-1} of water is shown in Fig. 4.10. The maximum and minimum temperatures of the segmented micro-channel heat sink are recorded at 57.8 ^{o}C and 54.8 ^{o}C, respectively. The variation of temperature across the novel segmented micro-channel heat sink is approximately 3.0 ^{o}C.

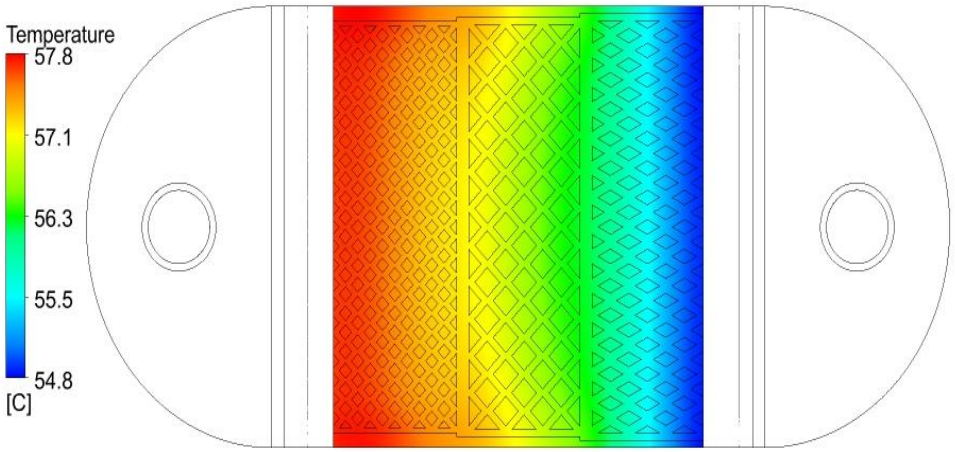

Fig 4.10 Temperature contour plot of the segmented micro-channel heat sink under 15 gs^{-1} of water

Pumping power needed for the segmented micro-channel heat sink under different mass flow rate is illustrated in Fig. 4.11. The pumping power is exponentially increasing with the mass flow rate of water. At a mass flow rate of 15 gs^{-1}, about 0.13 W of pumping power is needed.

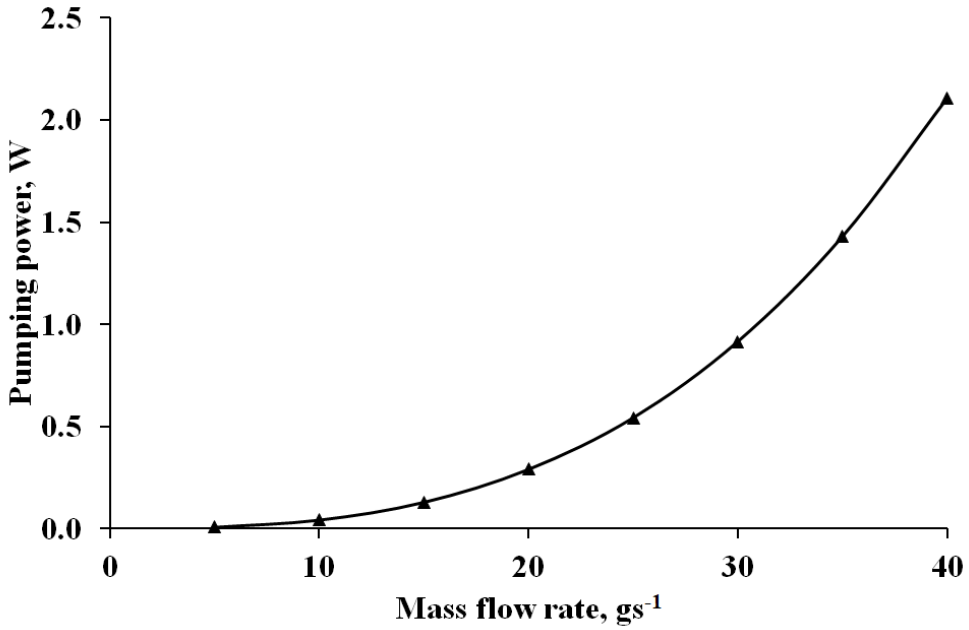

Fig 4.11 Pumping power needed for the segmented micro-channel heat sink under different mass flow rate

4.4 Comparison of segmented micro-channel with straight-channel

Comparison of the thermal resistance and variation of temperature for the segmented micro-channel and straight-channel heat sink are shown in Fig. 4.12 and Fig. 4.13, respectively. As shown in Fig. 4.12, thermal resistance for segmented micro-channel and straight-channel heat sink decreases with the inlet mass flow rate of water and the slope decreases gradually. This can be attributed to the reduction of convective thermal resistance. In comparison to the thermal resistance of straight-channel heat sink, the thermal resistance of the segmented micro-channel heat sink is comparatively lower. At 30 gs^{-1}, thermal resistances for the segmented micro-channel and straight-channel are 0.02589 and 0.08115, respectively. Hence, the thermal performance of the segmented micro-channel heat sink is threefold of the straight channel. A similar trend is also observed for the variation of temperature for the

segmented micro-channel and straight-channel heat sink. At 30 gs^{-1}, variations of temperature for the segmented micro-channel and straight-channel are 1.2 ^{o}C and 15.0 ^{o}C, respectively. The improvement in the variation of temperature is about 12.5 times of the straight channel. The effect of the mass flow rate on pressure drop is shown in Fig. 4.14. The pressure drop of the segmented micro-channel and straight-channel heat sink increases gradually with respect to the inlet mass flow rate of water. As compared to the pressure drop of the straight-channel heat sink, the pressure drop of the segmented micro-channel heat sink is comparatively higher. At 30 gs^{-1}, pressure drops of the segmented micro-channel heat sink is recorded at 30436 Pa, which is about 10 times higher than that of the straight-channel heat sink.

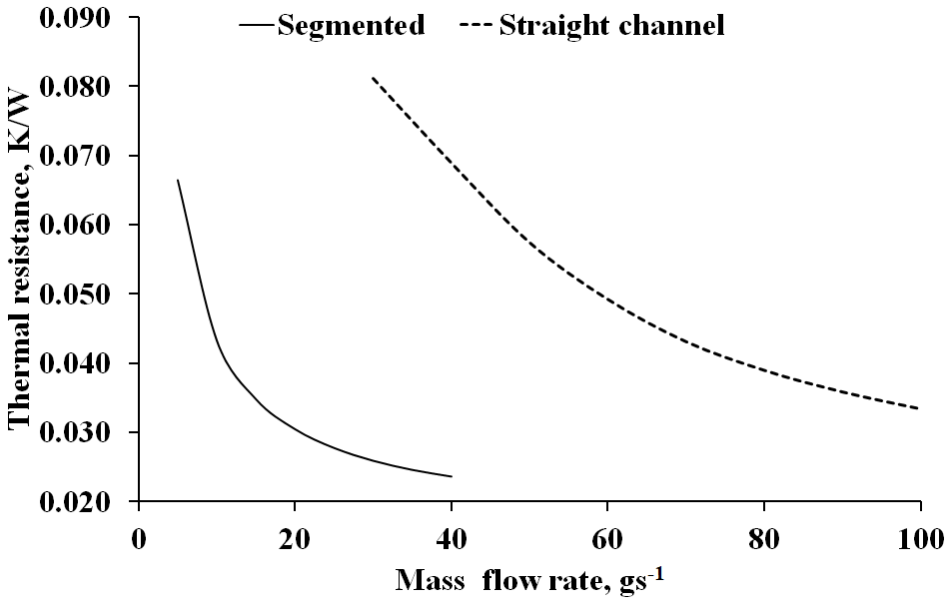

Fig 4.12 Comparison of the thermal resistance for the segmented micro-channel and straight-channel heat sink

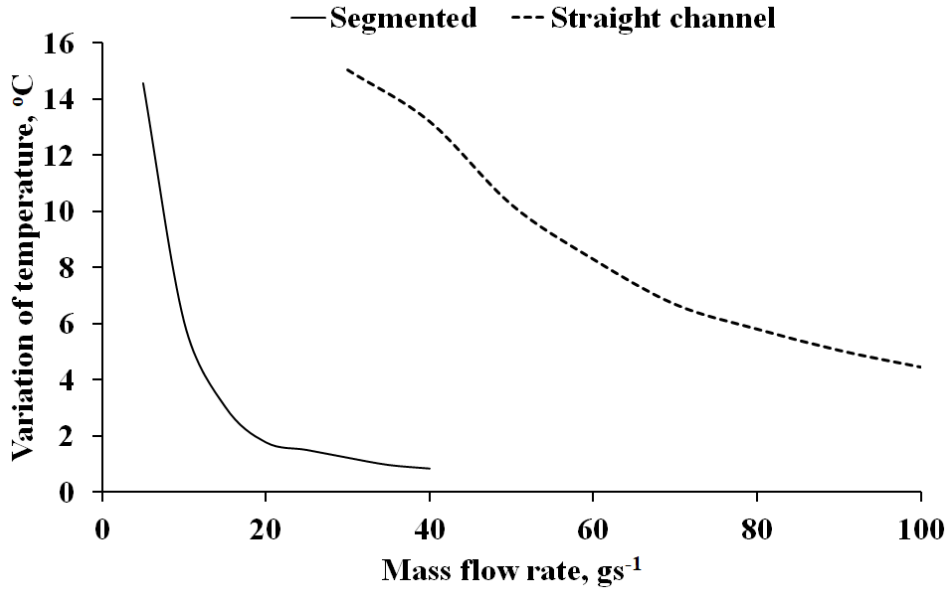

Fig 4.13 Comparison of variation of temperature for the segmented micro-channel and straight-channel heat sink

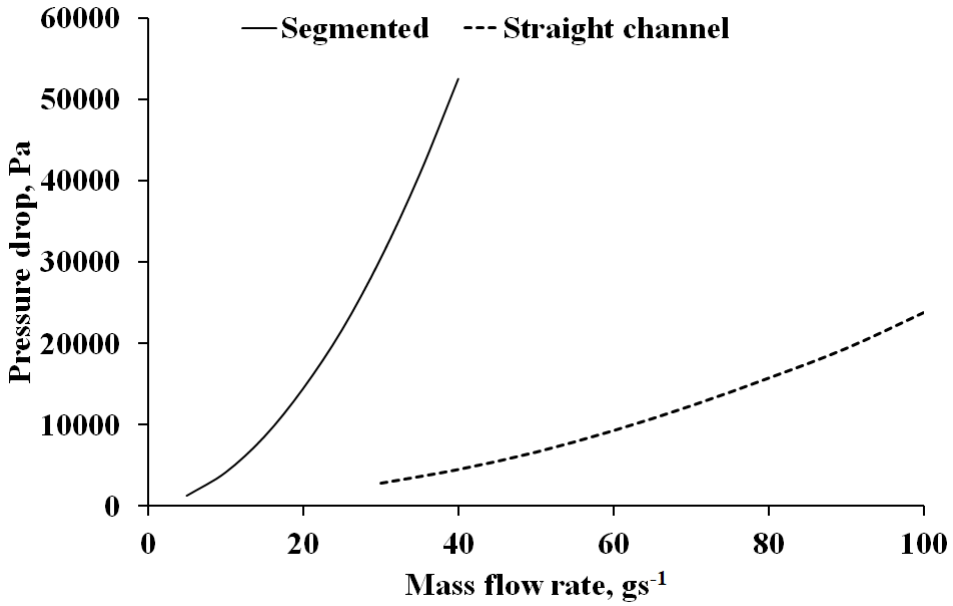

Fig 4.14 Effect of the mass flow rate on pressure drop

4.5 Experimental correlation

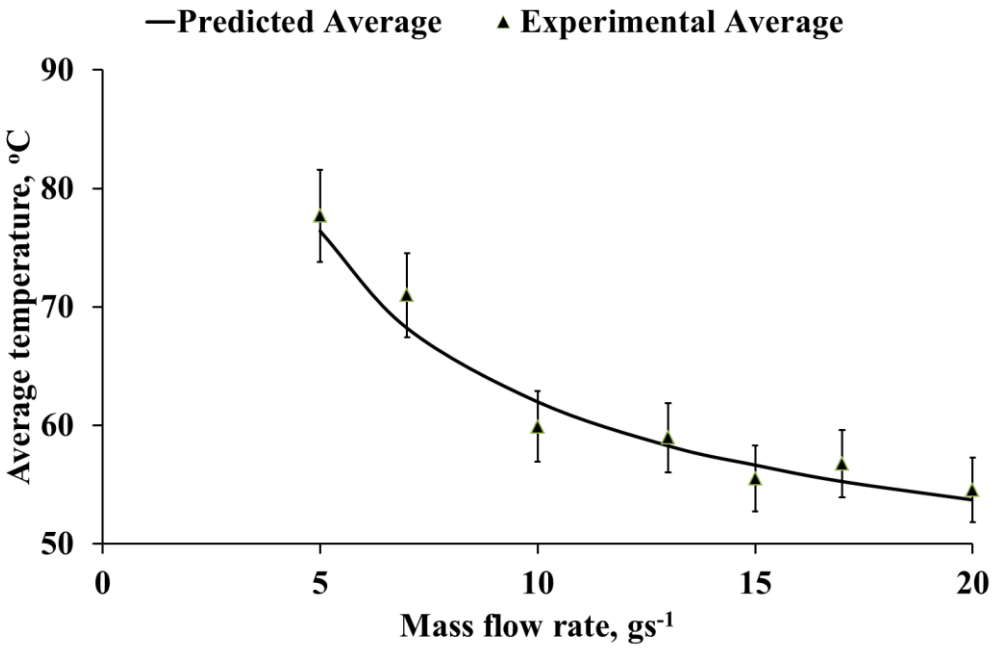

Fig 4.15 Average temperature comparison between experimental and simulation result

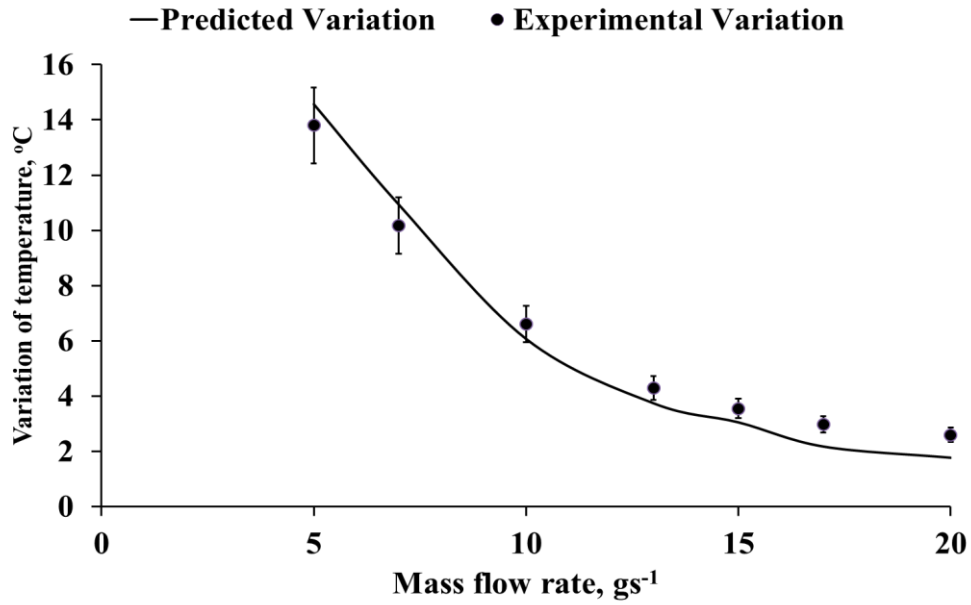

Fig 4.16 Temperature variation comparison between experimental and simulation result

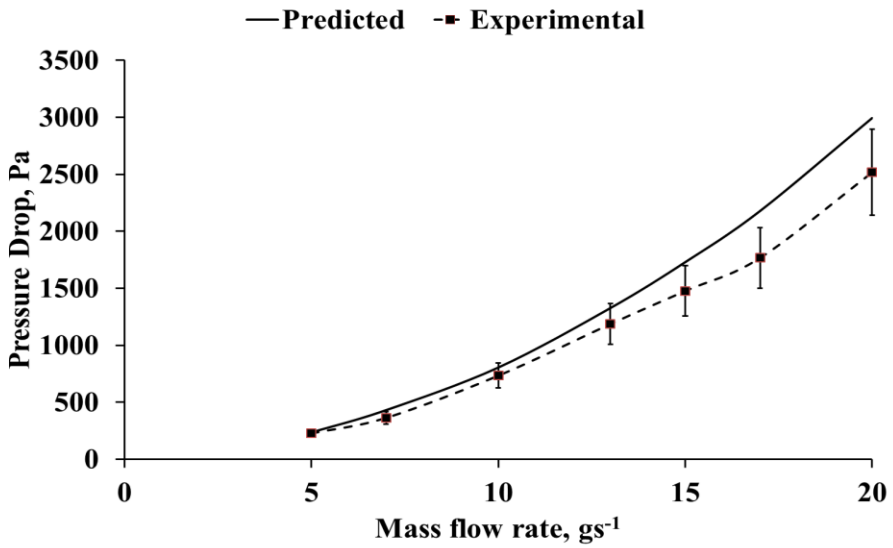

Fig 4.17 Pressure drop comparison between experimental and simulation result

The simulation results show that segmented fin micro-channel is capable of dissipating high heat flux compared to the conventional straight channel with a minimum variation of temperature and pumping power. This will provide an alternative solution for thermal management for high heat flux generated electronic devices. However, simulation results required validation with the experimental data. Fig 4.15, Fig 4.16 and Fig 4.17 show the comparison of experimental data with simulation results for average temperature, a variation of temperature and pressure drop respectively. The average temperature and variation of the temperature of the segmented micro-channel show a decreasing trend with the increase mass flow rate. On the other hand, the pressure drop across the segmented micro-channel shows an increasing trend with the mass flow rate of the cooling fluid. At a mass flow rate of 15 gs^{-1}, average temperature, temperature variation, and pressure drop are 55.5 ^{o}C, 3.6 ^{o}C and 1467 Pa respectively. The average error of the average temperature, variation of temperature and pressure drop 1.6%, 0.5%, and 84% respectively.

4.6 Summary

In this chapter, a comparison of the simulation results and experimental data has been conducted. It is clearly shown that the novel micro-channel heat sink has the ability to dissipate high heat flux and the thermal performance is far better than the conventional straight channel heat sink. Other than that, the segmented channel developed in this research work is able to reduce the variation of temperature and average temperature with minimum pumping power. Further evidence for the excellent thermal performance of the segmented micro-channel heat sink with lower cost. In the next chapter, the performance of the novel micro-channel will be discussed in details.

CHAPTER 5

DISCUSSION

5.1 Introduction

In this chapter, the performance of the segmented micro-channel heat sink is discussed in details and compared with previous studies on the straight micro-channel. The first section will discuss the comparison with the correlation of straight channel with previous research. Next, the performance of the straight channel heat sink and segmented micro-channel heat sink are compared to justify the strength and weaknesses of the segmented micro-channel compared to a straight channel.

5.2 Straight channel comparison with correlation

Correlation of Nusselt number versus Reynolds number and friction factor versus Reynolds number are derived from the regression analysis and can be expressed by Eq. 5-1 and Eq. 5-2, respectively.

$$Nu = 0.0435\, Re^{0.7318}\, Pr^{1/3} \quad (5\text{-}1)$$

$$f = 0.256\, Re^{-0.227} \quad (5\text{-}2)$$

Thermal management using mini-channel and micro-channel as the cooling solution in the electronic devices has attracted great attention from researchers recently. In liquid cooling, the conventional physical and mathematical correlations describing the heat transfer and fluid flow in the conventional channel can be applied on the micro-channel and mini-channel for small variations of surface roughness and wall thickness. Thus, the Nusselt number of the simulation results can be compared with Colburn, Dittus-Boelter, Sieder-Tate, and Gnielinski correlation as shown in Eq. 5-3, Eq. 5-4, Eq. 5-5 and Eq. 5-6, respectively (Incropera et al. 2007).

$$\mathrm{Nu} = 0.023\ \mathrm{Re}^{4/5}\ \mathrm{Pr}^{1/3} \tag{5-3}$$

$$\mathrm{Nu} = 0.023\ \mathrm{Re}^{4/5}\ \mathrm{Pr}^{0.4} \tag{5-4}$$

$$Nu = 0.027\ Re^{4/5}\ Pr^{1/3}\ \left(\frac{\mu}{\mu_s}\right)^{0.14} \tag{5-5}$$

μ Fluid viscosity at the bulk fluid temperature, $\mathrm{kg.m^{-1}.s^{-1}}$

μ_s Fluid viscosity at the heat-transfer boundary surface temperature, $\mathrm{kg.m^{-1}.s^{-1}}$

$$Nu = \frac{(f/8)\ (Re_D - 1000)\ Pr}{1 + 12.7\ (f/8)^{1/2}\ (Pr^{2/3} - 1)} \tag{5-6}$$

On the other hand, the friction factor of the simulation results can be compared with Blasius and Petukhov correlation as shown in Eq. 5-7 and Eq. 5-8, respectively (Incropera et al. 2007).

$$f = 0.3164\ \mathrm{Re}^{-0.25} \tag{5-7}$$

$$f = (0.790\ ln\ \mathrm{Re} - 1.64)^{-2} \tag{5-8}$$

Fig. 5.1 and Fig. 5.2 illustrate the comparison results of Nusselt number and friction factor, respectively. The average differences of Nusselt number for Colburn, Dittus-Boelter, Sieder-Tate, and Gnielinski correlations as compared to the simulation results are about 3.4 %, 9.0 %, 13.4 % and 2.5 %, respectively, as shown in Fig. 5.1. Among all correlations, Colburn correlation is in a good agreement with each other with an average difference of 3.4 %. On the hand, the average differences in the friction factor for Blasius and Petukhov correlations as compared to the simulation results are about 0.5 % and 1.9 %, respectively, as demonstrated in Fig. 5.2. The large deviation is found when the flow rate is about 30 gs^{-1} near to transition region while the conventional correlations are valid for the fully developed region. In addition, the test section used for conventional correlations is circular while the test section used in this study is rectangular. Therefore, a slight variation is expected for the simulation results and conventional correlations. In short, simulation results correlate well with the conventional correlations for Nusselt number and friction factor. CFD simulation of the heat sink has shown to be useful in providing insights of the different flow phenomenon and it offers a clear physical understanding of the heat transfer and flows field of the heat sink which is difficult to obtain through experimental works.

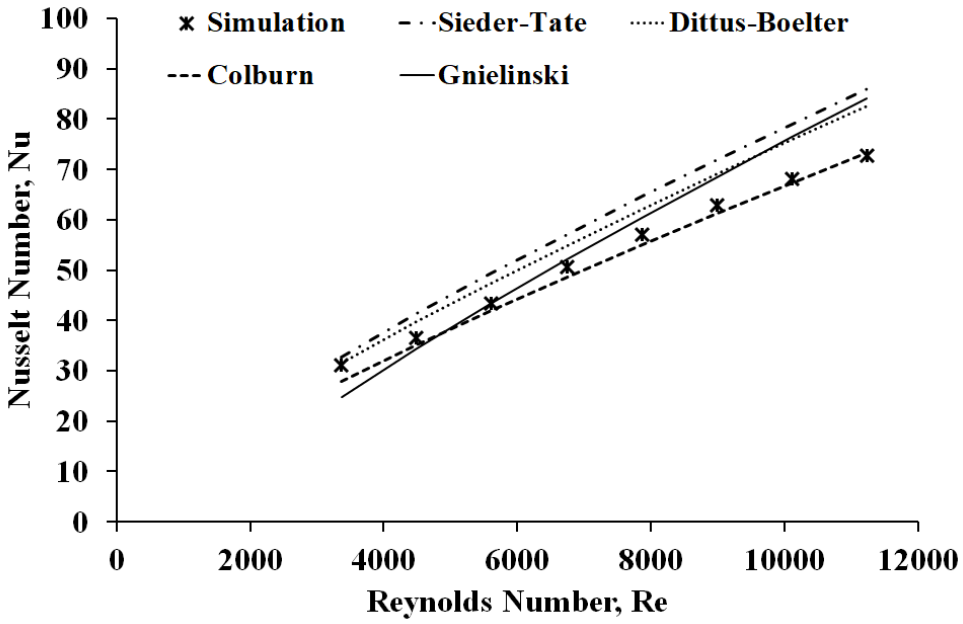

Fig 5.1 Average differences of Nusselt number for Colburn, Dittus-Boelter, Sieder-Tate and Gnielinski

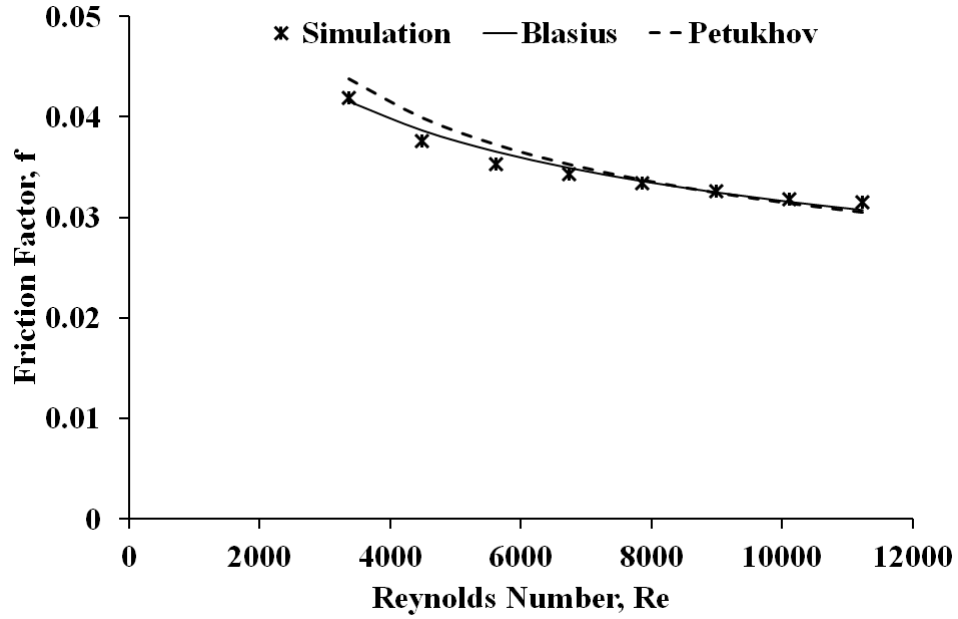

Fig 5.2 Average differences in the friction factor for Blasius and Petukhov correlations

5.3 Optimization

Considering the novel micro-channel heat sink design, it needs to be optimized in order to produce a better thermal performance. In this research, optimization was conducted using Taguchi-Grey analysis which eases the optimization procedure with lower cost and more efficient. Instead of using full factorial design, the Taguchi method is able to produce a better solution at minimum cost and time by creating 27 runs only compared to 726 runs with a full factorial design for six three-level factors. (Taguchi. 1987). From the simulation result, the optimized design shows that the micro-channel can dissipate heat load better than the conventional straight micro-channel heat sink. The optimum parameter for micro-channel heat sink is identified through Taguchi optimization with fin width of 1 mm, fin length of 2 mm, fin transverse distance of 1 mm, segmented number of 3 and flow rate of 15 gs^{-1}. Moreover, the optimized design of the segmented micro-channel heat sink showed that it can perform better than conventional straight micro-channel with lower pumping power.

The geometrical design is one of the most influential parameters in thermal performance. In the segmented micro-channel heat sink, the design parameters such as fin dimension, channel width and a number of segments are changed gradually and this evolution will alter the flow behavior in the micro-channel. A fluid mixing and re-initialization of the thermal boundary layer are the two main activities occurred in the segmented micro-channel heat sink. A fluid mixing and thermal boundary redevelopment will help in

promoting more uniform temperature distribution across the heated surface. Hence, the thermal performance of the segmented micro-channel heat sink is better than that of the straight channel. Furthermore, as the number of segments increases, the flow channel width is reduced and the number of fins present in the downstream is also increased. Chai et al. have conducted a series of numerical analysis to investigate the flow and heat transfer characteristics of an interrupted micro-channel heat sink by installing different configurations of ribs in the transverse micro-chambers (Chai et al. 2016). Based on the simulation results obtained, it is demonstrated that the heat transfer performance of an interrupted micro-channel heat sink is comparatively greater than that of a straight- channel heat sink owing to the enhanced heat transfer coefficient through fluid mixing and re-initialization of the thermal boundary layer in the micro-channel heat sink.

From the simulation result, it is clearly shown that the segmented micro-channel heat sink is capable to improve the thermal performance tremendously with lower pumping power, i.e. about 18 times less than that of the straight-channel heat sink. Based on the conjugate heat transfer analysis, correlation of Nusselt number versus Reynolds number and friction factor versus Reynolds number derived from the regression analysis are defined in Eq. 5-9 and Eq. 5-10, respectively. The Nusselt number and friction correlations can be used in the preliminary design of the cooling solution for the high heat load devices such as electronic chips, solar cell, an electric vehicle controller, laser gun, etc.

$$Nu = 2.468\ Re^{0.256}\ \mathrm{Pr}^{1/3} \quad (5\text{-}9)$$

$$f = 3.159\ Re^{-0.205} \quad (5\text{-}10)$$

For the electronic cooling, a minimum variation of temperature is the priority consideration. In order to achieve a variation of temperature less than 5 ^{o}C, straight-channel heat sink requires mass flow rate at least 100 gs^{-1} with a pressure loss of 23733 Pa. On the other hand, segmented micro-channel heat sink only requires a mass flow rate of 15 gs^{-1} with only 8522 Pa of pressure drop, which is 2.8 times less than the straight-channel heat sink. In short, the optimized structure of the segmented micro-channel heat sink provides excellent thermal performance as compared to the straight-channel heat sink with minimum energy consumption.

5.4 Comparison between the straight channel and segmented channel

Although straight channel has been used commercially, researchers still conducting experiments and simulation to improve its thermal performance. The maximum temperature and variation of temperature are two important criteria in the micro-channel heat sink design so that it can satisfy the stringent requirement set by ITRS which is 85 ^{o}C and less than 5 ^{o}C respectively. The simulation result proved that straight channel and segmented micro-channels heat sinks can be used to dissipate high heat flux. However, the efficiency of the thermal performance for the straight channel drops sharply approaching downstream as shown in Fig 4.2. Cooling efficiency of the straight micro-

channel is decreased along the channel flow path, which subsequently leads to a large temperature difference between upstream and downstream of the heated surface. On the other hand, segmented micro-channel heat sink introduces a gradual change of the fin size and flow channel width will further improve the thermal performance of the micro-channel heat sink. Gradually change of the fin and flow channel width will disrupt the development of the thermal boundary layer. In the straight channel, the geometric design allowed the thermal boundary to fully developed along the channel while in the segmented micro-channel design, the segmented section along the flow path creates a disturbance which allows the thermal boundary break up. This disturbance is similar to the vortex created inside the wavy channel to improve the thermal performance. However, in the wavy channel, certain hot spot produces due to the mal-distribution of the flow inside the micro-channel if it is not carefully designed. Thus, the introduction of the segmented channel helps in improving the thermal performance with better flow distribution. From the results in section 4.4, it is clearly shown that the thermal performance for novel segmented micro-channel heat sink is better than the straight channel heat sink.

5.5 Experimental analysis

From the experimental results in section 4.5, it is clearly shown that simulation and experimental correlate well for average temperature and variation of temperature with a relative error less than 5% at a mass flow rate of 15 gs^{-1}. The average temperature is about 55.5 ^{o}C which is less than 85 ^{o}C

as highlighted by ITRS. Meanwhile, the pressure drop result shows that when the flow rate increasing, the deviation of 84% is observed. This is due to leakage of the test rig at high pressure.

5.6 Summary

This chapter discusses the result of the research work from the aspect of average temperature, temperature variation, pressure drop, and pumping power. Based on the discussion, the segmented micro-channel is proved to be an excellent thermal management candidate compared to the straight channel in terms of pumping power and thermal performance. Besides, the uniform heat transfer along the channel can be obtained from the segmented micro-channel heat sink with the introduction of the secondary flow and segmented zone. For this research work, the optimized segmented fin design proved to be an important parameter in affecting the thermal performance of the micro-channel heat sink.

CHAPTER 6

CONCLUSION

6.1 Conclusion

In this study, CFD simulation on the straight-channel and segmented micro-channel heat sink is conducted. The effects of various design parameters, such as fin width, fin length, fin transverse distance, number of segments, channel width and mass flow rate on the heat transfer and flow characteristics, are optimized using Taguchi-Grey method. The optimal parameters have been assigned to maximize the specific performance, minimize pressure drop and minimize variation of temperature in the micro-channel heat sink. The most important design parameters affecting the specific performance of the segmented micro-channel heat sink are flow rate, channel width, fin width and a number of segments. The maximum specific performance of the segmented micro-channel heat sink is found to be 15 gs^{-1} mass flow rate, 0.3 mm channel width, 2 mm fin width and 3 segments micro-channel. The most important design parameters affecting the pressure drop in the segmented micro-channel heat sink are fin width, flow rate, channel width, and fin length. The pressure drop in the segmented micro-channel heat sink can be effectively reduced by controlling these parameters. The minimum pressure drop of the segmented micro-channel heat sink are recorded with the use of 1 mm fin width, 0.010 kg s^{-1} mass flow rate, 1 mm channel width and 2

mm fin length. The most important design parameters affecting the variation of temperature in the segmented micro-channel heat sink are a number of segments, mass flow rate, and channel width and fin transverse distance. The variation of temperature across the segmented micro-channel heat sink can be effectively reduced by controlling these parameters. Minimum variation of temperature is observed using 3 segments micro-channel, 20 gs^{-1} mass flow rate, 1 mm channel width and 5 mm fin transverse distances. When all desired responses are taken into account together, grey relation analysis is applied to optimize the segmented micro-channel heat sink. Optimum results are obtained when 1 mm fin width, 2 mm fin length, 5 mm fin transverse distance, 3 segments micro-channel, 1 mm channel width and 15 gs^{-1} mass flow rate are applied. The heat transfer performance of the straight-channel is weakened along the flow direction. This is due to the continuous development of the thermal boundary layer and reduction of the cooling capacity of water. On the other hand, segmented micro-channel is able to enhance the overall cooling performance that is impossible to be achieved through the conventional straight-channel heat sink. Heat transfer enhancement of the segmented micro-channel can be attributed to the fluid mixing and frequent thermal boundary layer development at each fin. Furthermore, increasing the total heat transfer area will further improve the heat transfer performance in the downstream. Based on the findings obtained in this study, it can be concluded that segmented micro-channel heat sink is an alternative solution for a thermal management system in high heat load electronic devices with minimum pumping power consumption. Furthermore, experimental results correlate well with the simulation results with a relative error of 1.5% and 0.5 % for average

temperature and variation of temperature respectively. Hence conclude that the segmented micro-channel heat sink is a potential candidate to replace conventional straight channel heat sink for thermal management purpose.

6.2 Future Work

In designing the micro-channel heat sink, in order to improve the heat dissipation, further optimization can be considered which include the angle of the secondary entrance which in this research the angle is constant. By changing the angle, it might influence the fluid flow behavior. The changing of fluid flow behavior can further improve fluid mixing and re-initialize the thermal boundary layer. Other than that, the fin number can also be increased which can increase the surface contact in the heat transfer process. Nanofluids have proven to be one of the coolants that have the potential to replace the conventional liquid coolant. The ability to increase the heat transfer properties of the cooling fluid is proved to be very crucial for the thermal management solution nowadays.

REFERENCES

Abdoli, A., Jimenez, G. and Dulikravich, G.S., 2015. Thermo-fluid analysis of micro pin-fin array cooling configurations for high heat fluxes with a hot spot. *Int J Therm Sci*, 90, pp. 290-297.

Adewale, P., Vithanage, L.N. and Christopher, L., 2017. Optimization of enzyme-catalysed bio-diesel production from crude tall oil using Taguchi method. *Energy Covers Manag*, 154, pp. 81-91.

Ahmed, H.E. and Ahmed, M.I., 2015. Optimum thermal design of triangular, trapezoidal and rectangular grooved microchannel heat sinks. *Int Commun Heat Mass Transf*, 66, pp. 47-57.

Ahmed, H.E., Ahmed, M.I., Seder, I.M.F. and Salman, B.H., 2016. Experimental investigation for sequential triangular double-layered microchannel heat sink with nanofluids. *Int Commun Heat Mass Transf*, 77, pp. 104-115.

Ahmed, H.E., Salman, B.H., Kherbeet, A.S. and Ahmed, M.I., 2018. Optimization of thermal design of heat sink: a review. *Int J Heat Mass Trans*, 118, pp. 129-153.

Alfaryjat, A.A., Mohammed, H.A., Adam N.M., Ariffin M.K.A. and Najafabadi, M.I., 2014. Influence of geometrical parameters of hexagonal, circular, and rhombus microchannel heat sinks on the thermohydraulic characteristic. *Int Commun Heat Mass Transf*, 52, 121-131.

Alvarado, B.R., Li, P., Liu, H. and Guerrero, A.H., 2011. CFD study of liquid cooled heat sinks with microchannel flow field configurations for electronics, fuel cells, and concentrated solar cells. *Appl Therm Eng*, 31, pp. 2494-257.

Anys, 2010. *ANSYS CFX-Solver modeling guide*. Canonsburg:Ansys Inc.

Bardina, J.E., Huang, P.G. and Coakley, T.J., 1997. Turbulence modeling validation testing and development. Nasa Techn. Memor., 110446, pp. 1-15.

Brinda, R., Daniel, R.J. and Sumangala, K., 2012. Ladder shape microchannels employed high performance micro cooling system for ULSI. *Int J Heat Mass Transf*, 55, pp. 3400-3411.

Chai, L., Xia, G.D. and Wang, H.S., 2015. Numerical study of laminar flow and heat transfer in microchannel heat sink with offset ribs on sidewalls. *App Therm Eng*, 92, pp. 32-41.

Chai, L., Xia, G.D. and Wang, H.S., 2016. Laminar flow and heat transfer characteristic of interrupted microchannel heat sink with ribs in the transverse microchambers. *Int J Therm Sci*, 110, pp. 1-11.

Chai, L., Xia, G.D. and Wang, H.S., 2016. Parametric study on thermal and hydraulic characteristic of laminar flow microchannel heat sink with fan-shaped ribs on sidewalls – Part 3 Performance evaluation. *Int J Heat Mass Transf*, 97, pp. 1091-1101.

Che, Z., Wong, T.N., Nguyen, N.T. and Yang, C., 2015. Three dimensional features of convective heat transfer in droplet-based micro-channel heat sink. *Int J Heat Mass Transf*, 86, pp. 455-464.

Chen, C. and Ding, C., 2011. Study on the thermal behavior and cooling performance of nanofluid-cooled microchannel heat sink. *Int J Therm Sci*, 50, pp. 378-384.

Chen, W.H., Huang, S.R. and Lin, Y.L., 2015. Performance analysis and optimum operation of a thermoelectric generator by Taguchi method. *Appl Energy*, 158, pp. 44-54.

Chiam, Z.L., Lee, P.S., Singh, P.K. and Mou, N., 2016. Investigation of fluid flow and heat transfer in wavy micro-channel with alternating secondary branches. *Int J Heat Mass Transf*, 101, pp. 1316-1330.

Chingulpitak, S. and Wongwises, S., 2015. A review of effect of flow directions and behaviors on thermal performance of conventional heat sinks. *Int J Heat Mass Transf*, 81, pp. 10-18.

Chiu, H.C., Jang, J.H., Yeh, H.W. and Wu, M.S., 2011. The heat transfer characteristic of liquid cooling heatsink containing microchannel. *Int J Heat Mass Transf*, 54, pp. 34-42.

Cho, E.S., Choi, J.W., Yoon, J.S. and Kim, M.S., 2010. Modelling and simulation on the mass flow distribution in microchannel heat sinks with non-uniform heat flux conditions. *Int J Heat Mass Transf*, 53, pp. 1341-1348.

Chuan, L., Wang, X.D., Wang, T.H. and Yan, W.M., 2015. Fluid flow and heat transfer in microchannel heat sink based on porous fin design concept. Int Commun Heat Mass Transf, 65, pp. 52-57.

Colgan, E.G., Furman, B., Gayness, M., Graham, W.S., LaBianca, N.C., Magerlein, J.H. and et al., 2007. A practical implementation of silicon microchannel coolers for high power chips. *IEEE Trans Compon Packag Technol*, 30, pp. 218-225.

Deng, D., Wan, W., Shao, H., Tang, Y., Feng, J. and Zeng, J., 2015. Effects of operation parameters on flow boiling characteristic of heat sink cooling systems with re-entrant porous micro-channels. *Energy Convers Manag*, 96, pp. 340-351.

Deng, D., Wan, W., Tang, Y., Wan Z. and Liang, D., 2015. Experimental investigations on flow boiling performance of re-entrant and rectangular microchannel – a comperative study. *Int J Heat Mass Transf*, 82, pp. 435-446.

Dey, A., Debnath, S. and Pandey, K.M., 2017. Optimization of electrical discharge machining process parameters for Al6061/cenosphere composite using grey-based hybrid approach. *Trans. Nonferrous Met. Sco, China*, 27, pp. 998-1010.

Ebrahimi, A., Roohi, E. and Kheradmand, S., 2015. Numerical study of liquid flow and heat transfer in rectangular microchannel with longitudinal vortex generators. *Appl Therm Eng*, 78, pp. 576-583.

Ebrahimi, A., Rikhtegar, F., Sabaghan, A. and Roohi, E., 2016. Heat transfer and entropy generation in microchannel with longitudinal vortex generators using nanofluids. *Energy*, 101, pp. 190-201.

Fan, Y., Lee, P.S. and Chua, B.W., 2014. Investigation on the influence of edge effect on flow and temperature uniformities in cylindrical oblique-finned mini-channel array. *Int J Heat Mass Transfer*, 70, pp. 651-663.

Fan, Y., Lee, P.S., Jin, L.W. and Chua, B.W., 2013. A simulation and experimental study of fluid flow and heat transfer on cylindrical oblique-finned heat sinks. Int J Heat Mass Transf, 61, 62-72.

Fan, Y., Lee, P.S., Jin, L.W., Chua, B.W. and Zhang, D.C., 2014. A parametric investigation of heat transfer and friction characteristics in cylindrical oblique fin microchannel heat sink. *Int J Heat Mass Transf*, 68, pp. 567-584.

Ghale, X.Y., Haghshenasfard, M. and Esfahany, M.N., 2015. Investigation of nanofluids heat transfer in a ribbed microchannel heat sink using single-phase and multiphase CFD models. *Int Commun Heat Mass Transf*, 68, pp. 122-129.

Ghani, I.A., Kamaruzaman, N. and Sidik, N.A.C., 2017. Heat transfer augmentation in a microchannel heat sink with sinusoidal cavities and rectangular ribs. *Int J Heat Mass Transf*, 108, pp. 1969-1981.

Habib, M.A., Ul-Hag, I., Badr. H.M. and Said, S.A.M., 1998. Calculation of turbulent flow and heat transfer in periodically converging-diverging channels. *Comput Fluids*, 27, pp. 95-120.

He, H., Li, P., Yan, R. and Pan, L., 2016. Modeling of reversal flow and pressure fluctuation in rectangular microchannel. *Int J Heat Mass Transf*, 102, pp. 1024-1033.

Hung, T.C., Yan, W.M., Wang, X.D. and Huang, Y.X., 2012. Optimal design of geometric parameters of double-layered microchannel heat sinks. *Int J Heat Mass Transf*, 55, pp. 3262-3272.

Hung, T.C., Huang, Y.X. and Yan, W.M., 2013. Thermal performance analysis of porous microchannel heat sinks with different configuration design. *Int J Heat Mass Transf*, 66, pp. 235-243.

Incropera, F.P., Dewitt, D.P., Bergman, T.L. and Lavine, A., 2007. *A Fundamentals of Heat and Mass Transfer. 6th ed*. New York: John Wiley & Sons.

Jaikumar, A. and Kandlikar, S.G., 2015. Enhanced pool boiling for electronics cooling using porous fin tops on open microchannels with FC-87. *Appl Therm Eng*, 91, 426-433.

Jang, D., Yook, S.J. and Lee, K.S., 2014. Optimum design of radial heat sink with a fin-height profile for high power LED lighting application. *Appl Energy*, 116, pp. 260-268.

Jin, L.W., Lee, P.S., Kong, X.X., Fan, Y. and Chou, S.K., 2014. Ultra-thin minichannel LCP for EV battery thermal management. *Appl Energy*, 113, pp. 1786-1794.

Joshi, L.C., Singh, S. and Kumar, S.R., 2014. A review on enhancement of heat transfer in microchannel exchanger. *Int J Innov Sci Eng Technol*, 9, pp. 529-535.

Kays, W.M. and London, A.L., 1964. *Compact Heat Exchangers*, *2nd ed*. New York: McGraw-Hill.

Khan, J.A., Monjur Morshed, AKMM. and Fang, R., 2014. Towards ultra-compact high heat flux microchannel heat sink. *Procedia Eng*, 90, pp. 11-24.

Kotcioglu, I., Cansiz, A. and Khalaji, M.N., 2013. Experimental investigation for optimization of design parameters in rectangular duct with plate-fins heat exchanger by Taguchi method. Appl Therm Eng, 50, pp. 604-613.

Kuppusamy, N.R., Mohammed, H.A. and Lim, C.W., 2013. Numerical investigation of trapezoidal grooved microchannel heat sink using nanofluids. *Thermochim Acta*, 573, pp. 39-56.

Law, M. and Lee, P.S., 2015. A comperative study of experimental flow boiling heat transfer and pressure characteristic in straight and oblique-finned microchannels. *Int J Heat Mass Trans*, 85, pp. 797-810.

Lee, G.G., Allan, W.D.E. and Boulama, K.G., 2013. Flow and performance characteristics of an Allison 250 gas turbine S-shaped diffuser: effects of geometry variations. *Int J Heat Fluid Flow*, 42, pp. 151-163.

Lee, Y.J., Singh, P.K. and Lee, P.S., 2015. Fluid flow and heat transfer investigations on enhanced microchannel heat sink using oblique fins with parametric study. *Int J Heat Mass Transf*, 81, pp. 325-336.

Leng, C., Wang, X.D., Wang, T.H. and Yan, W.M., 2015. Optimization of thermal resistance and bottom wall temperature uniformity for double-layered microchannel heat sinks. *Energy Convers Manag*, 93, pp. 141-150.

Li, Y., Zhang, F., Sunden, B. and Xie, G., 2014. Laminar thermal performance of microchannel heat sink with constructal vertical Y-shaped bifurcation plates. *Appl Therm Eng*, 73, pp. 183-193.

Li, S.N., Zhang, H.N., Li, X.B., Li, Q., Li, F.C., Qian, S. and Joo, S.W., 2016. Numerical study on the heat transfer performance of non-Newtonian fluid in manifold microchannel heat sink. *Appl Therm Eng*, 115, pp. 1213-1225.

Li, Y.F., Xia, G.D., Ma, D.D., Jia, Y.T. and Wang, J., 2016. Characteristic of laminar flow and heat transfer in microchannel heat sink with triangular cavities and rectangular ribs. *Int J Heat Mass Transf*, 98, pp. 17-28.

Lie, X.L, Tao, W.Q. and He, Y.L., 2007. Numerical study of turbulent heat transfer and pressure drop characteristics in a water-cooled minichannel heat sink. *Trans ASME-J Elec Pack*, 129, pp. 247-255.

Lin, L., Chen, Y.Y., Zhang, X.X. and Wang, X.D., 2014. Optimization of geometry and flow rate distribution for double-layered microchannel heat sink. *Int J Therm Sci*, 78, pp. 158-168.

Ma, D.D., Xia, G.D., Li, Y.F., Jia, Y.T. and Wang, J., 2016. Effects of structural parameters on fluid flow and heat transfer characteristic in microchannel with offset zigzag grooves in sidewall. *Int J Heat Mass Transf*, 101, pp. 427-435.

Menter, F.R., Kuntz, M. and Langtry, R., 2003. *Ten years of industrial experience with SST turbulence model*. Turbulence, Heat and Mass Transfer, 4th ed., US: Begell House.

Mohammadian, S.K., He, Y.L. and Zhang, Y., 2015. Internal cooling of lithium-ion battery using electrolyte as coolant through microchannels embedded inside the electrodes. *J Power Sources*, 293, pp. 458-466.

Mohammed, H.A., Gunnasegaran, P. and Shuaib, N.H., 2011. Numerical simulation of heat transfer enhancement in wavy microchannel heat sink. *Int Commun Heat Mass Transf*, 38, pp. 63-68.

Mou, N., Lee, P.S. and Khan, S.A., 2016. Coupled equivalent circuit models for fluid flow and heat transfer in larger connected microchannel networks – the case of oblique fin heat exchanger. *Int J Heat Mass Transf*, 102, pp. 1056-1072.

Naqiuddin, N.H., Saw, L.H., Yew, M.C., Yusof, F., Ng, T.C., Yew, M.K., 2018. Overview of micro-channel design for high heat flux application. *Renewable and Sustainable Energy Reviews*, 82, pp. 901-914

Naqiuddin, N.H., Saw, L.H., Yew, M.C., Yusof, F., Poon, H.M., Cai, Z., Thiam, H.S., 2018. Numerical investigation for optimizing segmented micro-channel heat sink by Taguchi-Grey method. *Applied Energy*, 222, pp. 437–450

Pandey, N., Murugesan, K. and Thomas, H.R., 2017. Optimization of ground heat exchanger for space heating and cooling applications using Taguchi method and utility concept. *Appl Energy*, 1890, pp. 421-438.

Peng, X.F. and Peterson, G.P., 1995. The effect of thermalfluid and geometrical parameters on convection of liquids through rectangular microchannels. *Int J Heat Mass Transf*, 38, pp. 755-758.

Peyghambarzadeh, S.M., Hashemabadi, S.H., Chabi, A.R. and Salimi, M., 2014. Performance of water based CuO and Al_2O_3 nanofluids in Cu-Be alloy heat sink with rectangular microchannel. *Energy Convers Manag*, 119, pp. 28-38.

Prajapati, Y.K., Pathak, M. and Khan, M.K., 2016. Transient heat transfer characteristic of segmented finned microchannels. *Exp Therm Fluid Sci*, 79, pp. 134-142.

Priesnitz, B.H., MuChen, Z. and Gao, J., 2016. Influence of geometric parameters on flow and heat transfer performance of microchannel heat sink. *Appl Therm Eng*, 107, pp. 870-879.

Radwan, A., Ahmed, M. and Ookawara, S., 2016. Performance enhancement of concentrated photovoltaic system using a microchannel heat sink with nanofluids. *Energy Convers Manag*, 119, pp. 289-303.

Raghuraman, D.R.S., Raj, R.T.K., Nagarajan, P.K. and Rao, B.V.A., 2016. Influence of aspect ratio on the thermal performance of rectangular shaped micro channel heat sink using CFD code. *Alex Eng J*, 56, pp. 43-54.

Rahman, M.M., 2000. Measurements of heat transfer in microchannel heat sink. *Int Commun Heat Mass Transf*, 27, pp. 495-506.

Riofrio, M.C., Caney, N. and Gruss, J.A., 2016. State of the art of efficient pumped two-phase flow cooling technologies. *App Therm Eng*, 104, pp. 333-343.

Rostami, J., Abbassi, A. and Saffar-Avval, M., 2015. Optimization of conjugate heat transfer in wavy walls microchannel. *Appl Therm Eng*, 82, pp. 318-328.

Ross, P.J., 1996. *Taguchi Techniques for Quality Engineering*. New York: McGraw-Hill.

Roy, R.K., 2001. *Design of Experiments using the Taguchi Approach: 16 Steps to Product and Process Improvement*. New York: John Wiley & Sons Inc.

Rubio-Jimenez, C.A., Hernandez-Guerrero, A., Cervante, J.G., Lorenzini-Gutierrez, D. and Gonzalez-Valle, C.U., 2016. CFD study of constructal microchannel networks for liquid-cooling of electronic devices. *Appl Therm Eng*, 95, pp. 374-381.

Sahin, B., Yakut, K., Kotcioglu, I. and Celik, C., 2005. Optimum design parameters of heat exchanger. *Appl Energy*, 82, pp. 90-106.

Saw, L.H., Ye, Y., Tay, A.A.O., Chong, W.T., Kuan, S.H. and Yew, M.C., 2016. Computational fluid dynamic and thermal analysis of Lithium-ion battery pack with air cooling. *Appl Energy*, 177, pp. 783-792.

Saw, L.H., Ye, Y., Yew, M.C., Chong, W.T., Yew, M.K. and Ng, T.C., 2017. Computational fluid dynamics simulation on open cell aluminium foams for Li-ion battery cooling system. *Appl Energy*, 204, pp. 1489-1499.

Sakanova, A., Yin, S., Zhao, J., Wu, J.M. and Leong, K.C., 2014. Optimization and comparison of double-layer and double-side micro-channel heat sinks with nanofluid for power electronic cooling. *Appl Therm Eng*, 65, pp. 124-134.

Sakanova, A., Keian, C.C. and Zhao, J., 2015. Performance of microchannel heat sink using wavy microchannel and nanofluids. *Int J Heat Mass Transf*, 89, 59-74.

Sandhya, D., Mekala, C.S.R. and Veeredhi, V.R., 2016. Improving the cooling performance of automobile radiator with ethylene glycol water based TiO_2 nanofluids, *Int Commun Heat Mass Transf*, 78, pp. 121-126.

Selvam, C., Mohan Lal, D. and Harish, S., 2016. Thermal conductivity enhancement of ethylene glycol and water with grapheme nanoplatelets. *Termochim Acta*, 642, pp. 32-38.

Shafeie, H., Abouali, O., Jafarpur, K. and Ahmadi, G., 2013. Numerical study of heat transfer performance of single-phase heat sinks with micro pin-fin structures. *Appl Therm Eng*, 58, pp. 68-76.

Sharma, G.S., Schlottig, G., Brunschwiler, T., Tiwari, M.K., Michel, C. and Poulikakos, D., 2015. A novel method of energy efficient hotspot-targeted embedded liquid cooling for electronics and experimental study. *Int J Heat Mass Transf*, 2015, pp. 684-694.

Sharman, G.S., Tiwan, M.K., Zimmermann, S., Brunschwiler, T., Schlotting, G., Michel, B. and et al., 2015. Energy efficient hotspot-targeted embedded liquid cooling of electronics. *Appl Energy*, 138, pp. 414-422

Siva, V.M., Pattamatta, A. and Das, S.K., 2014. Effect of flow maldistribution on the thermal performance of parallel microchannel cooling systems. *Int J Heat Mass Transf*, 73, pp. 424-428.

Smith, E.M., 2005. *Advances in thermal design of heat exchangers*. Chichester, West Sussex, England: John Wiley & Sons, Ltd.

Soltanimehr, M. and Afrand, M., 2016. Thermal conductivity enhancement of COOH-funtionalized MWCNTs/ethylene glycol water nanofluid for application in heating and cooling system. *Appl Therm Eng*, 105, pp. 716-723.

Sparrow, E.M., Abraham, J.P. and Minkowycz, W.J., 2009. Flow separation in a diverging conical duct: effect of Reynolds number and divergence angle. *Int J Heat Mass Transfer*, 52, pp. 3079-3083.

Srikanth, R., Nemani, P. and Balaji, C., 2015. Multi-objective geometric optimization of a PCM based matrix typr composite heat sink. *Appl Energy*, 156, pp. 703-714.

Taguchi, G., 1987. *Taguchi Techniques for Quality Engineering*. New York: Quality resources.

Thiangtham, P., Keepainboon, C., Kiatpachai, P., Asirvatham, L.G., Mahian, O., Dalkilic, A.D. and Wongwises, S., 2016. An experimental study on two-phase flow patterns and heat transfer characteristics during boiling of R134a flowing through a multi microchannel heat sink. *Int J Heat Mass Transf*, 98, 390-400.

Tran, N., Chang, Y.J., Teng, J.T., Dang, T. and Greif, R., 2016. Enhancement thermodynamic performance of microchannel heat sink by using a novel multi-nozzle structure. *Int J Heat Mass Transf*, 101, pp. 656-666.

Tsai, C.H., Chang, C.L. and Chen, L., 2003. Applying grey relational analysis to the vendor evaluation model. *Int J Comp, Intern Manag*, 11, pp. 45-53.

Vajravelu, K. and Sastri, K.S., 1980. Natural convective heat transfer in vertical wavy channels. *Int J Heat Mass Transf*, 23, pp. 408-411.

Vieser, W., Esch, T. and Menter, F., 2002. *Heat transfer predictions using advanced two equation turbulence models*. CFX validation Report.

Wang, B.X. and Peng, X.F., 1994. Experimental investigation on liquid forced-convection heat transfer through microchannels. *Int J Heat Mass Transf*, 37, pp. 73-82.

Wang, G., Niu, D., Xie, F., Wang, Y., Zhao, X. and Ding, G., 2015. Experimental and numerical investigation of a microchannel heat sink (MCHS) with micro-scale ribs and grooves for chip cooling. *Appl Therm Eng*, 85, 61-70.

Wang, H., Chen, Z. and Gao, J., 2016. Influence of Geometric Parameters on flow and heat transfer performance of micro-channel heat sink. *Appl Therm Eng*, 107, pp. 870-879.

Wong, K.C. and Lee, J.H., 2015. Investigation of thermal performance of micro-channel heat sink with triangular ribs in the transverse microchambers. *Int Commun Heat Mass Transf*, 65, pp. 103-110.

Wong, K.C. and Muezzin, F.N.A., 2013. Heat transfer of a parallel flow two-layered microchannel heat sink. *Int Commun Heat Mass Transf*, 49, pp. 136-140.

Wu, H.H., 1996. *The Introduction of Grey Analysis*. Taipei: Gauli Publishing Co.

Wu, J., Zhao, J., Lei, J. and Liu, B., 2016. Effectiveness of nanofluid on improving the performance of microchannel heat sink. *Appl Therm Eng*, 101, pp. 402-412.

Wu, Z., Caliot, C., Bai, F., Flamant, G., Wang, Z., Zhang, J. and et al., 2010. Experimental and numerical studies of the pressure drop in ceramic foams for volumetric solar receiver applications. *Appl Energy*, 87, pp. 504-513.

Xia, G., Ma, D., Zhai, Y., Li, Y. and Du, M., 2015. Experimental and numerical study of fluid flow and heat transfer characteristic in microchannel heat sink with complex structure. *Energy Convers Manag*, 105, pp. 848-857.

Xia, G.D., Jiang, J., Wang, J., Zhai, Y.L. and Ma, D.D., 2015. Effects of different geometric structures on fluid flow and heat transfer performance in microchannel heat sinks. *Int J Heat Mass Transf*, 80, pp. 439-447.

Xia, G.D., Liu, R., Wang, J. and Du, M., 2016. The characteristic of convective heat transfer in microchannel heat sink using Al_2O_3 and TiO_2 nanofluids. *Int Commun Heat Mass Transf*, 76, pp. 256-264.

Xie, G., Shen H. and Wang, C., 2015. Parametric study in thermal performance of microchannel heat sinks with internal vertical Y-shaped bifurications. *Int J Heat Mass Transf*, 90, pp. 948-958.

Xu, M., Lu, H., Chai, J.C. and Duan, X., 2016. Parametric numerical study of the flow and heat transfer in microchannel with dimples. *Int Commun Heat Mass Transf*, 76, pp. 348-357.

Yan, Y., Yan, H., Yin, S., Zhang, L., Li, L., 2019. Single/multi-objective optimizations on hydraulic and thermal management in micro-channel heat sink with bionic Y-shaped fractal network by genetic algorithm coupled with numerical simulation. *International Journal of Heat and Mass Transfer*, 129, pp. 468-479

Yang, Y.T., Tang, H.W., Zeng, B.Y. and Wu, C.H., 2015. Numerical simulation and optimization of turbulent nanofluids in three-dimensional rectangular rib-grooved channel. *Int Commun Heat Mass Transf*, 66, pp. 71-79.

Yang, Y.T., Tsai, K.T., Wang, Y.H. and Lin, S.H., 2014. Numerical study of microchannel heat sink performance using nanofluids. *Int Commun Heat Mass Transf*, 57, pp. 27-35.

Yin, L., Xu, R., Jiang, P., Cai, H. and Jia, L., 2017. Subcooled flow boiling of water in a large aspects ratio microchannel. *Int J Heat Mass Transf*, 112, pp. 1081-1089.

Yue, Y., Shahebeddin, S., Mohammadian, K. and Zhang, Y., 2015. Analysis of performances of manifold microchannel heat sink with nanofluids. *Int J Therm Sci*, 89, pp. 305-313.

Zhai, Y.L., Xhia, G.D., Liu X.F. and Li, Y.F., 2015. Energy analysis and performance evaluation of flow and heat transfer in different micro heat sinks with complex structure. *Int J Heat Mass Transf*, 84, pp. 293-303.

Zhai, Y., Xia, G., Chen, Z. and Li, Z., 2016. Micro-PIV study of flow and the formation of vortex in micro heat sinks with cavities and ribs. *Int J Heat Mass Transf*, 98, pp. 380-389

Appendix A

Summarization for all design of micro-channel

Reference	Method	Type of micro-channel	Heat source	Type of coolant
Khan et al., 2014	Experiment	Straight channel	7.7 $MW.m^{-2}$	Water
Gong et al., 2015	Computational	Straight channel, pin fin, single hole jet cooling, double layer	1.0 $MW.m^{-2}$	Water
Brinda et al., 2012	Computational	Ladder shape	2.5 $MW.m^{-2}$	Water
Abdoli et al., 2015	Computational	Micro pin fin	20.0 $MW.m^{-2}$	Water
Chen and Ding, 2011	Experiment	Porous straight channel	7.9 $MW.m^{-2}$	Al_2O_3 - H_2O
Xia et al., 2015	Experiment and simulation	Straight channel and staggered complex corrugated channel	6.2 $MW.m^{-2}$	Water
Zhai et al., 2015	Computational	Triangular cavities with circular rib, Triangular cavities with triangular rib, Triangular cavities with trapezoidal rib, Trapezoidal cavities with circular rib, Trapezoidal cavities with triangular rib, Trapezoidal cavities with trapezoidal rib	1.0 $MW.m^{-2}$	Water

Sharma et al., 2015	Experiment	Manifold micro-channel	3.0 $MW.m^{-2}$	-
He et al., 2016	Modelling	Straight channel	42.6 $MW.m^{-2}$	Water
Raghuraman et al., 2016	Computational	Straight channel	21.5 $MW.m^{-2}$	Water
Chai et al., 2016	Computational	Straight channel, rectangular rib, backward triangular rib, diamond rib, forward triangular rib and ellipsoidal rib	1.0 $MW.m^{-2}$	Water
Chai et al., 2015	Computational	Offset ribs (rectangular, backward triangular, isosceles, triangular, forward triangular and semi-circular)	1.0 $MW.m^{-2}$	Water
Chai et al., 2016	Computational	Fan-shaped ribs	1.0 $MW.m^{-2}$	Water
Li et al., 2014	Computational	Straight channel and Y-shaped bifurcation	3.0 $MW.m^{-2}$	Water
Sakanova et al., 2015	Computational	Straight channel and wavy channel	1.0 $MW.m^{-2}$	Water
Ma et al., 2016	Computational	Straight channel and zigzag channel	2.0 $MW.m^{-2}$	Water
Shafeie et al., 2013	Computational	Micro pin fin	1.7 M $W.m^{-2}$	Water
Ghani et al., 2017	Computational	Sinusoidal cavities and rectangular rib	1.0 $MW.m^{-2}$	-

Li et al., 2016	Computational	Triangular cavities and rectangular rib	1.0 $MW.m^{-2}$	Water
Wang et al., 2016	Computational	Rectangular, trapezoidal and triangular shaped	1.0 $MW.m^{-2}$	Water
Xu et al., 2016	Computational	Dimples	1.0 $MW.m^{-2}$	Water
Colgan et al., 2007	Experiment	Staggered fin and continuous fin	2.75 $MW.m^{-2}$	Water
Priesnitz et al., 2016	Computational	porous medium with rectangular, outlet enlargement, trapezoidal, thin rectangular, block and sandwich distribution	1.0 $MW.m^{-2}$	Water
Xia et al., 2015	Computational	Straight channel, offset fan-shaped re-entrant cavities, triangular re-entrant cavities	2.0 $MW.m^{-2}$	Water
Leng et al., 2015 Lin et al., 2014, Wong and Muezzin, 2013, Hung et al., 2012	Computational	Double-layered micro-channel	1.0 $MW.m^{-2}$	Water
Tran et al. 2016	Computational	Multi-nozzles	2.0 $MW.m^{-2}$	Water

Chuan et al. 2015	Computational	Porous fin	1.0 $MW.m^{-2}$	Water
Wong and Lee 2015	Computational	Triangular ribs	1.2 $MW.m^{-2}$	Water
Ahmed and Ahmed, 2015	Computational	Triangular, trapezoidal and rectangular grooved	1.0 $MW.m^{-2}$	Water
Wang et al. 2015	Computational	Micro-scale ribs and grooves	1.0 $MW.m^{-2}$	Water
Sakanova et al. 2014	Computational	Double layer and double side	2.0 $MW.m^{-2}$	Al_2O_3-H_2O
Kuppusamy et al. 2013	Computational	Trapezoidal grooved	1.0 $MW.m^{-2}$	Al_2O_3-H_2O
Wu et al. 2016	Computational	Straight channel	2.0 $MW.m^{-2}$	Al_2O_3-H_2O Cu-H_2O Cu-Al_2O_3-H_2O AlN-H_2O AlN-Al_2O_3-H_2O Si-H_2O Si-Al_2O_3-H_2O
Xia et al. 2016	Computational	Straight channel	2.0 $MW.m^{-2}$	Water, Al_2O_3-H_2O TiO_2-H_2O